UNIVERSITÀ
DI PAVIA

Dipartimento di Biologia e Biotecnologie
"Lazzaro Spallanzani"

Laurea Magistralis in Molecular Biology and Genetics

SINGLE-CELL AND FUNCTIONAL CHARACTERISATION OF TUMOUR-INFILTRATING B CELLS ACROSS BLADDER CANCER STAGES

Supervisor:
Prof. Luca Vangelista

Co-supervisor (s), if any:
Prof. Diletta Di Mitri

Experimental
thesis by
Giacomo Bettolini

Academic Year 2025/2026

UNIVERSITÀ
DI PAVIA

Dipartimento di Biologia e Biotecnologie
"Lazzaro Spallanzani"

Laurea Magistralis in Molecular Biology and Genetics

SINGLE-CELL AND FUNCTIONAL CHARACTERISATION OF TUMOUR-INFILTRATING B CELLS ACROSS BLADDER CANCER STAGES

CARATTERIZZAZIONE FUNZIONALE E A SINGOLA CELLULA DEI LINFOCITI B INFILTRANTI IL TUMORE NEI DIVERSI STADI DEL CARCINOMA VESCICALE

Supervisor:
Prof. Luca Vangelista

Co-supervisor (s), if any:
Prof. Diletta Di Mitri

Experimental
thesis by
Giacomo Bettolini

Academic Year 2025/2026

SINGLE-CELL AND FUNCTIONAL CHARACTERISATION OF TUMOUR-INFILTRATING B CELLS ACROSS BLADDER CANCER STAGES

Bladder cancer is among the most common malignancies worldwide and carries high rates of recurrence and progression. The shift from non-muscle-invasive (NMIBC) to muscle-invasive disease (MIBC) marks a decisive change in clinical trajectory, yet the immunological events that accompany it, and that perhaps allow it, remain only partially defined. Within the immune infiltrate, this is even more the case for B cells, whose contribution to anti-tumour immunosurveillance is less studied than that of T cells and of the myeloid compartment. In this work, we therefore characterised at high resolution the immune profile of bladder cancer across the transition from non-muscle-invasive to muscle-invasive disease, and determined whether the alterations observed in patients could be reproduced experimentally and attributed to tumour-derived soluble factors. We performed single-cell RNA sequencing on tumour tissue from a cohort of 73 enrolled patients, from which we processed 9 NMIBC, 8 MIBC and 2 benign papillomas. Global clustering was followed by dedicated reclusterings of the major immune populations, alongside differential gene expression, pathway enrichment and inferred cell-cell communication analyses. We then assessed the effect of the tumour secretome by exposing murine splenic B cells to conditioned medium from the MB49 bladder cancer cell line, both under resting conditions and in the presence of stimuli driving plasma cell differentiation, and finally we employed the BBN carcinogen-induced mouse model, with analyses at an early (week 16) and at a late (week 24) time point. Reclustering of the myeloid and T/NK lymphoid compartments returned frequency differences consistent with the literature, which, being purely compositional measures, do not in themselves allow the conclusion that these populations are functionally different between the two stages. The B cell compartment also showed substantial variations: in MIBC the fraction of non-terminally differentiated B cells was higher than in NMIBC, with a corresponding decrease in the plasma cell to non-plasma cell ratio, suggesting a defect in plasma cell differentiation specific to invasive disease. Transcriptional analysis supported this reading, showing downregulation of JCHAIN, of B cell receptor signalling and of N-linked glycosylation in MIBC. Ligand-receptor analysis further revealed an increase in signalling directed from tumour cells towards the plasma cell and plasmablast clusters. *In*

vitro, conditioned medium induced a marked increase in CXCR4 on B cells, the most pronounced alteration observed in the experiment, and significantly hindered LPS-induced plasma cell differentiation. Re-examining the patient dataset, we confirmed that B cells are the population showing the strongest CXCR4 upregulation in MIBC. In the BBN model, treated mice at the late time point showed a reduction in mature B cells and in plasma cells relative to controls, consistent with an impairment of B cell differentiation affecting multiple maturation stages. Taken together, three independent systems converge in indicating that B cell differentiation is impaired at multiple levels in muscle-invasive disease, and above all at the transition to plasma cells, accompanied by downregulation of the transcriptional programmes required for immunoglobulin assembly and secretion. CXCR4 emerges as the most prominent candidate associated with this phenotype: its upregulation in patient B cells, its strong induction by conditioned medium, and the existence of a published mechanism whereby dysregulated CXCR4 signalling arrests plasma cell maturation at immature stages support the hypothesis of an initiated but incomplete differentiation programme, at present supported by association rather than by causal evidence.

CARATTERIZZAZIONE FUNZIONALE E A SINGOLA CELLULA DEI LINFOCITI B INFILTRANTI IL TUMORE NEI DIVERSI STADI DEL CARCINOMA VESCICALE

Il carcinoma della vescica è tra le neoplasie più frequenti a livello mondiale ed è gravato da elevati tassi di recidiva e progressione. Il passaggio dalla forma non muscolo-invasiva (NMIBC) a quella muscolo-invasiva (MIBC) segna un cambiamento decisivo nella traiettoria clinica, ma gli eventi immunologici che lo accompagnano, e che forse lo permettono, restano solo parzialmente definiti. All'interno dell'infiltrato immunitario questo vale in misura ancora maggiore per le cellule B, il cui contributo all'immunosorveglianza antitumorale è meno studiato rispetto a quello dei linfociti T e del compartimento mieloide. In questo lavoro abbiamo quindi caratterizzato ad alta risoluzione il profilo immunitario del carcinoma vescicale lungo la transizione dalla malattia non muscolo-invasiva a quella muscolo-invasiva, e verificato se le alterazioni osservate nei pazienti fossero riproducibili sperimentalmente e attribuibili a fattori solubili di origine tumorale. Abbiamo eseguito un sequenziamento dell'RNA a singola cellula su tessuto tumorale proveniente da una coorte di 73 pazienti arruolati, dalla quale abbiamo processato 9 NMIBC, 8 MIBC e 2 papillomi benigni. Al clustering globale abbiamo fatto seguire reclustering dedicati alle principali popolazioni immunitarie, affiancati da analisi di espressione genica differenziale, di arricchimento dei pathway e di comunicazione cellulare inferita. Abbiamo poi valutato l'effetto del secretoma tumorale esponendo cellule B spleniche murine a terreno condizionato della linea di carcinoma vescicale MB49, sia in condizioni basali sia in presenza di stimoli differenzianti verso la plasmacellula, e infine abbiamo impiegato il modello murino di carcinogenesi indotta da BBN, con analisi a un timepoint precoce (settimana 16) e a uno tardivo (settimana 24). I reclustering dei compartimenti mieloide e linfoide T/NK hanno restituito differenze di frequenza coerenti con la letteratura, che tuttavia, in quanto misure puramente compositive, non permettono di per sé di concludere che tali popolazioni siano funzionalmente diverse tra i due stadi. Anche il compartimento B ha mostrato variazioni sostanziali: nel MIBC la frazione di cellule B non terminalmente differenziate risulta superiore rispetto al NMIBC, con un corrispondente calo del rapporto plasmacellule/non plasmacellule, suggerendo un difetto di differenziazione verso la plasmacellula specifico della malattia invasiva. L'analisi funzionale ha sostenuto questa lettura, mostrando nel MIBC la downregolazione di JCHAIN, del signalling del recettore delle cellule B e della

glicosilazione N-legata. L'analisi delle interazioni ligando-recettore ha inoltre evidenziato un aumento del segnale diretto dal tumore verso i cluster plasmacellulari e plasmablastici. *In vitro*, il terreno condizionato ha indotto un marcato aumento di CXCR4 sulle cellule B, l'alterazione più pronunciata osservata nell'esperimento, e ha ostacolato significativamente la differenziazione plasmacellulare indotta da LPS. Riesaminando il dataset dei pazienti, abbiamo confermato che le cellule B sono la popolazione con la più forte upregolazione di CXCR4 nel MIBC. Nel modello BBN, i topi trattati al timepoint tardivo hanno mostrato una riduzione delle cellule B mature e delle plasmacellule rispetto ai controlli, in linea con un'alterazione della differenziazione B che interessa più stadi maturativi. Nel complesso, tre sistemi indipendenti convergono nell'indicare che la differenziazione delle cellule B è compromessa a più livelli nella malattia muscolo-invasiva, e in primo luogo nella transizione a plasmacellula, accompagnata dalla downregolazione dei programmi trascrizionali necessari all'assemblaggio e alla secrezione delle immunoglobuline. CXCR4 emerge come il candidato più rilevante associato a questo fenotipo: la sua upregolazione nelle cellule B dei pazienti, la sua forte induzione da parte del terreno condizionato e l'esistenza di un meccanismo pubblicato per cui un signalling di CXCR4 disregolato arresta la maturazione plasmacellulare a stadi immaturi sostengono l'ipotesi di un programma differenziativo iniziato ma incompleto, al momento supportata da associazione più che da evidenza causale.

Table of contents

INTRODUCTION

1. Bladder histology

The urinary bladder is a distensible, hollow, muscular organ which serves as a temporary reservoir for urine. Urine is continuously produced by the kidneys through blood filtration and represents the primary route for the elimination of metabolic byproducts and xenobiotics from the circulation[1]. Following its excretion, urine is transported via the ureters through coordinated contractions until it reaches the bladder, where it is stored until voluntary micturition occurs[1]. Histologically, the bladder wall consists of four layers, from outermost to innermost: serosa, a muscular layer of the detrusor muscle, lamina propria, urothelium[1]. Urine is collected in the lumen, the internal space of the bladder[1]. The serosa is a thin connective tissue layer that covers the bladder dome, which is the upper part of the bladder, and it is continuous with the peritoneal layer of the abdominal wall. It also contains blood vessels of various sizes[2]. In the areas where there is no serosa, the bladder is instead covered by the adventitia (**FIG.1**), a loose connective tissue layer[2]. The walls of the bladder are primarily formed by detrusor muscle (**FIG.1**), a smooth muscle under the control of the autonomic system, which allows the bladder to either contract to excrete urine or relax to hold urine[1]. The lamina propria is a supporting layer of connective tissue that contains capillaries, lymphatic vessels, and neuroreceptors. It is demarcated from the urothelium by a distinct basement membrane[1] (**FIG.1**). The urothelium is a stratified, transitional epithelium that lines the renal pelvis, ureters, bladder, and proximal urethra and plays an important barrier role, preventing absorption of toxic substances carried by urine and defending against pathogen entry from the external environment[3]. The urothelium consists of three cell types: basal, intermediate, and superficial cells, which can also be referred to as umbrella cells or facet cells (**FIG. 2**). The basal cells are positioned along the basement membrane and are the smallest cells in the urothelium.

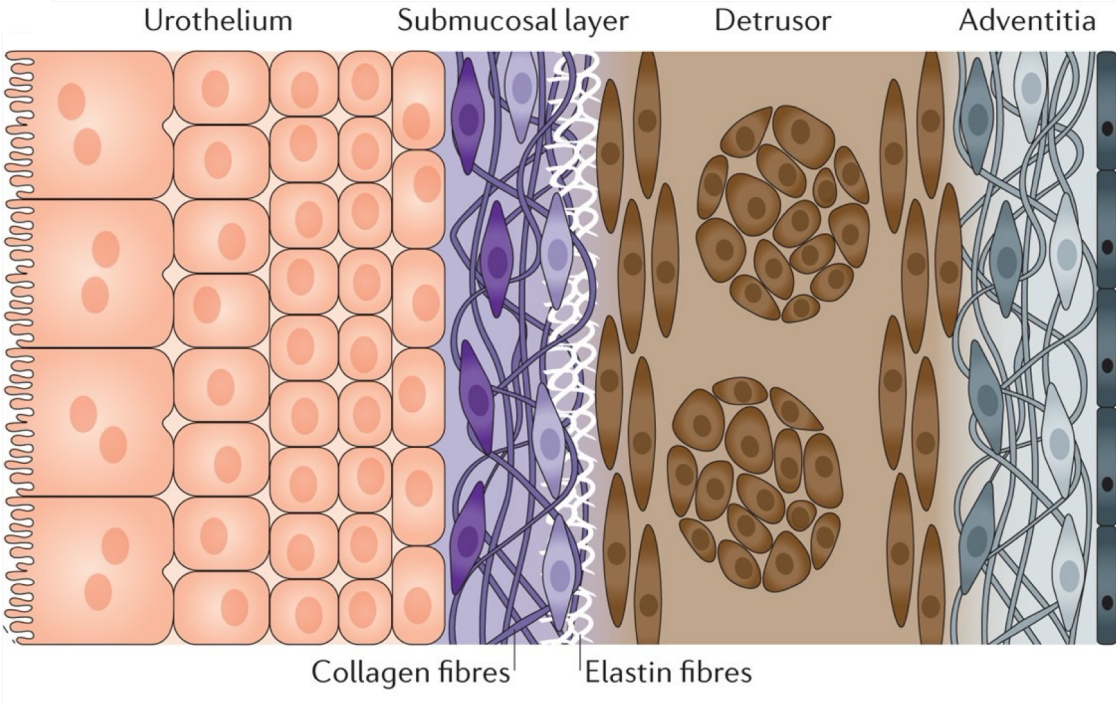

***FIG. 1* Histological layers of the bladder wall.** The layers are shown from outermost on the right to innermost to the left. Collagen fibres are shown in the adventitia and in the submucosal layer as long strings spanning the tissue. The detrusor muscle layer is shown with the longitudinal muscle layers adjacent to the adventitia and to the submucosal layer, and with the circular muscle in the central section. The submucosal layer, also called lamina propria, is interwoven with elastin fibers, which give the bladder wall the ability to distend and recoil. *Ajalloueian et al., 2018.*

They are distinguished by the expression of high levels of cytokeratin-5 (CK5), p63, and Sonic hedgehog (Shh)[4]. Additionally, recent literature points out how some bladder basal cells display stem cell properties, sustaining epidermal growth and renewal (**FIG.2**), both *in vitro* and *in vivo*[5], similarly to what is observed for other stratified epithelial cells. Directly above the basal cells, it's possible to find intermediate cells organized in thick layers[6] (**FIG.2**). They can be distinguished from basal cells based on their diameter and on the differential expression of several genetic markers, including uroplakins (UPK[6]), similarly to umbrella cells, from which they differ based on their expression of p63[6]. The outermost layer of the urothelium consists of highly differentiated umbrella cells, which line the lumen and play a critical role in maintaining the urinary barrier[6] (**FIG.2**). These terminally differentiated, specialized cells are large, hexagonal in shape, highly polarized, and can range from 25 to 250 μm in diameter, depending on bladder distension level[7]. In the relaxed state, they form a dome-shaped structure at the apical pole and can extend over several underlying intermediate cells, similarly to an umbrella[7]. This peculiar configuration is progressively lost upon bladder distension and filling, as these cells

undergo marked expansion and flattening to accommodate tissue stretching (distended state)[7]. Furthermore, independently of the state they are in, umbrella cells are the sole cells capable of forming both tight junctions and adherens junctions, and seal the intercellular space between adjacent cells, maintaining the integrity of the urothelial barrier throughout bladder filling and voiding cycles [8]. This barrier function is further reinforced with the presence of uroplakins. In humans, umbrella cells synthesize UPK1A, UPK1B, UPK2, and UPK3A, four major uroplakins[9]. These transmembrane proteins assemble into a hexagonal crystalline lattice at the apical membrane, establishing high electrical resistance and impermeability, which in turn regulate water and ion passage from the urine to the underlying tissue[9].

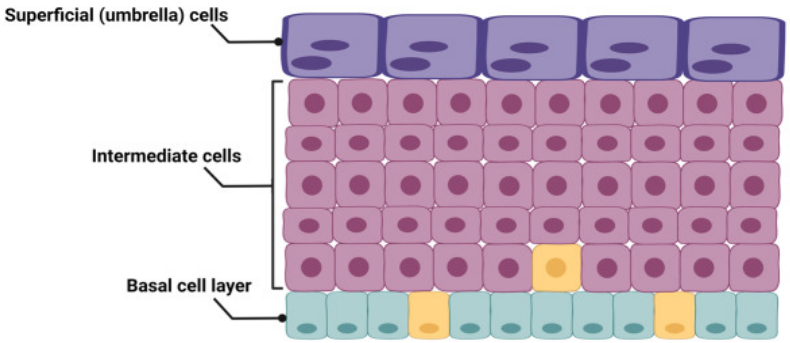

	Stem cells	Basal cells	Intermediate cells	Umbrella cells
CK5	++++	++++	+/–	–
CK14	++++	+/–	–	–
CK20	–	–	–	++++
P63	++++	++++	+++	–
Shh	++++	++++	++++	–
UPK	–	–	+/–	++++

***FIG.2* Urothelial cell layers and molecular markers.** The figure represents the organization of the healthy urothelium. From top to bottom, the umbrella cell layer is shown, then the thick intermediate cell layer, and finally the basal cell layer. The urothelial stem cells are also shown in yellow in the deeper layers, closer to the lamina propria. In addition, the expression of the distinctive markers for these populations is reported in the table under the representation of the tissue. *Jafari and Rohn, 2022*

2. Bladder cancer

2.1 Bladder cancer epidemiology

Bladder cancer is currently recognized as a major contributor to global cancer deaths, especially among men. In 2022, an estimated 614298 new cases of bladder cancer were diagnosed worldwide, making it the ninth most frequently diagnosed cancer globally[10]. In the same year, 220596 deaths were attributed to bladder cancer, ranking it as the thirteenth leading cause of cancer-related mortality worldwide, with around 75% of cases and deaths being men[10](**FIG.3**). Moreover, this malignancy exhibits a strong age-related pattern, with both incidence and mortality remarkably increasing with advancing age[11]. The highest incidence and mortality rates for bladder cancer in 2022 by world region were observed in southern Europe (incidence of 28,7 for males and 7 for females; mortality of 6,1 for males and 1,3 for females), with Italy and Spain having the highest incidence rates for males (31,5 and 33,8, respectively) and Netherlands and Italy having the highest incidence rates for females (7,9 and 6,5, respectively)[10]. The highest mortality rates are instead found in eastern Europe, with Poland and Hungary having the highest mortality rates for males (8,2 and 6,9, respectively), and females (1,5 and 2,0, respectively)[10](**FIG.3**). The differences in incidence rate between males and females lie in the risk factors for bladder cancer, among which age represents the principal non-modifiable risk factor[12]. In the US, 90% of diagnoses are made in individuals older than 55 years, and 80% in those older than 65 years, with the average age at diagnosis of 73 years[12]. Tobacco smoking is the main preventable risk factor, accounting for approximately 50-65% of new cases each year[12]. Tobacco smoke contains multiple known carcinogens, including beta-naphthylamine and polycyclic aromatic hydrocarbons[12]. The second greatest environmental risk factor for bladder cancer is occupational exposure to carcinogens, like aromatic amines, polycyclic aromatic hydrocarbons, and chlorinated hydrocarbons[12]. High-risk occupational categories include workers in petroleum products industries, firefighters, and hairdressers[12]. Overall, occupational exposure is estimated to be the cause of 18% of bladder cancer cases[12]. Finally, dietary habits have been shown to contribute to the risk of bladder cancer onset[12]. Obesity has been associated with an increased risk of 10% compared to normal weight[12]. Having regard to the information above, the higher incidence in males can be largely

attributed to the historically greater exposure to tobacco use and occupational carcinogens[13]. Since the great majority of bladder cancer cases are sporadic rather than hereditary, preventable risk factors are the major players in its aetiology[13]. For this reason, bladder cancer represents an optimal candidate for public health prevention interventions, including smoking cessation initiatives, implementation of occupational safety measures, dietary modification and weight management, which could all significantly reduce disease incidence[14].

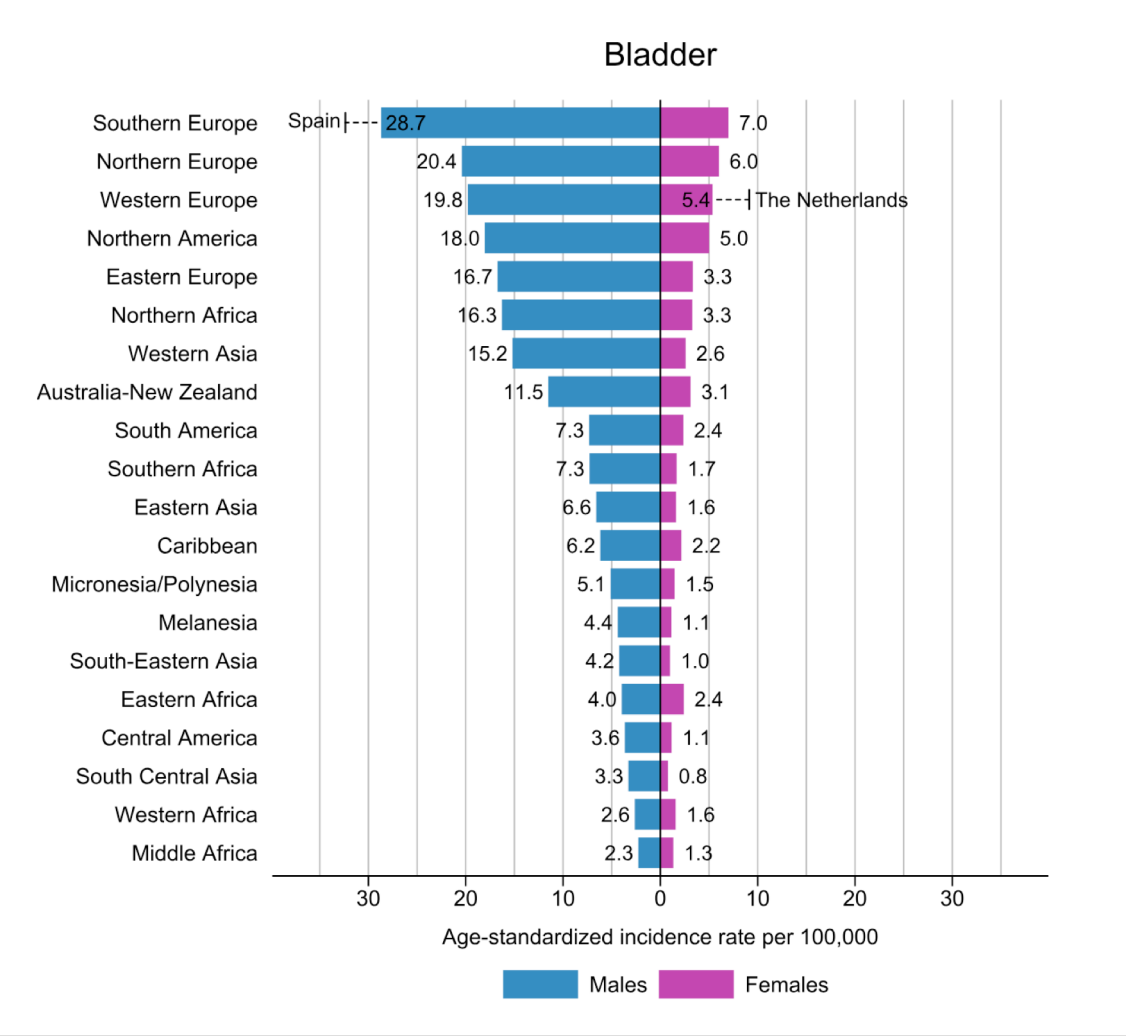

FIG. 3. **Bladder cancer incidence rates.** Bar chart of the region-specific age-standardized incidence rate by sex for bladder cancer in 2022. Rates are in descending order of incidence rate among males. The countries with the highest incidence rates among males and females are highlighted within the region they belong to. *Bray et al., 2024.*

2.2 Bladder cancer development and staging

Bladder cancer has been associated with field cancerization, a concept first described by Slaughter et al. in 1953 and defined as the acquisition of pro-tumorigenic mutations and genomic alterations within histologically normal-appearing cell lineages. These studies also suggest a monoclonal origin of such fields. When a stem cell acquires a genetic alteration, all progeny within the resulting clonal patch will inherit the same mutation, generating a genetically altered field[15]. Over time, additional genetic and epigenetic events may accumulate within this field, promoting malignant transformation. Consequently, distinct but clonally related tumours can arise in the same region, leading to the development of a second primary tumour after surgical removal of the initial lesion, rather than a recurrence due to incomplete resection[16]. In the context of bladder cancer, Krt14-expressing stem cells represent the only identified stem cell population associated with this phenomenon[17]. In particular, exposure to externally derived carcinogens transported in the urine causes their expansion, leading to field formation and neoplastic transformation[17]. This mechanism provides a biological explanation for the strong impact of lifetime exposure to environmental toxins on bladder cancer development. Bladder cancer is categorized according to the standardized Tumour Nodes Metastasis (TNM) staging system, which was developed by the American Joint Committee on Cancer (AJCC), into non-muscle-invasive bladder cancer (NMIBC), comprehending the early stages Tis, Ta and T1); muscle-invasive bladder cancer (MIBC), including stages T2, T3 and T4, defined by detrusor muscle invasion; or metastatic bladder cancer, spread to sites distant from the bladder[18] (**FIG. 4**). This classification of the disease is primarily used to guide treatment decisions, as the therapeutic approaches differ significantly between these categories[19,20].

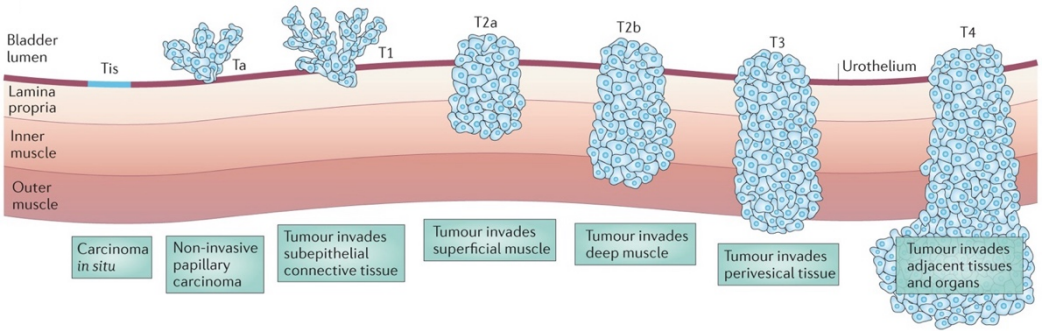

***FIG. 4*. Bladder cancer stages classification.** Bladder cancer stages are organized based on the presence or absence of detrusor muscle invasion, in non-muscle-invasive bladder cancer (NMIBC), comprehending stages Tis, Ta, and T1, and muscle-invasive bladder cancer (MIBC), including late stages T2, T3, and T4, characterized by detrusor muscle invasion. (Knowles and Hurst, 2014)

NMIBC and MIBC are organized into three stages each, based on the depth of tissue invasion[18]. The first of the two possible earlier stages of bladder cancer is known as Carcinoma *in situ* (CIS, also called Tis) (**FIG. 4**), belonging to the NMIBC group, and is characterized by flat, disordered proliferation of urothelial cells with marked cytologic abnormalities on the tissue lining the inside of the bladder[21]. Although it has non-invasive features, CIS is the main precursor of invasive carcinoma, since up to 83% of patients with urothelial CIS will develop invasive carcinoma[21]. Furthermore, the majority of urothelial CIS patients also present with papillary urothelial carcinoma[21]. Approximately 80% of bladder tumours present themselves as the second one of the possible earlier stages of bladder cancer: non-muscle-invasive superficial papillary lesions (Ta)[22] (**FIG. 4**), and include benign urothelial papilloma and malignant papillary urothelial carcinoma (PUC). Although papilloma and PUC share morphological similarities, looking like long, thin growths extending into the bladder lumen, they differ in treatment options and expected clinical outcomes[23]. Papilloma is considered a benign disease with low risk of relapse and a potential for malignancy, whereas PUC is a malignant condition that may necessitate invasive treatment or surveillance[23]. Ta tumours are relatively stable, with only 10-15% eventually progressing to invasive carcinoma[22]. The intrinsic difference in malignant potential between CIS and Ta lesions is codified in the histological grading system, which simultaneously reflects the biological behaviour and provides an estimate of the progression risk for Ta tumours. In particular, cancer grade describes how abnormal the cancer cells look under a microscope (atypia) and serves as a predictor for biological aggressiveness[24]. In 2004, the World Health Organization (WHO) adopted a binary

grading system for urothelial carcinoma, categorizing tumours as either low-grade or high-grade, based on their histopathological features, including structural abnormalities of the tissues, cytological atypia, and mitotic activity[25]. According to this grading system, CIS is always high-grade, while Ta lesions may be either low-grade or high-grade, depending on their genetic alterations. Ta lesions display gain-of-function mutations in the oncogenes HRAS, FGFR3, and PI3K, while CIS and invasive tumours show frequent loss-of-function mutations in the tumour suppressor genes TP53 and RB, and their related pathways[26]. Moreover, CIS and invasive bladder cancer display a higher chromosomal instability compared to Ta[27]. Ta tumours, as well as CIS tumours, may progress into their associated invasive phenotype (Stage I bladder cancer, T1), due to additional alterations in the p53 pathway[26]. Stage I bladder cancer (T1) (**FIG. 4**), whether of Ta or CIS origin, is defined by the invasion of the lamina propria while remaining confined above the muscular layers of the bladder[28]. Despite being included in the non–muscle-invasive group, it shares many of its genetic features with MIBC[29]. As a result, high-grade T1 tumours are at risk of both undertreatment and overtreatment. Undertreatment may occur when these tumours are managed according to conventional NMIBC protocols rather than being considered for early cystectomy, despite their aggressive biological behaviour[30]. Conversely, overtreatment may arise when cystectomy is performed in patients whose tumours lack the features that justify such a radical intervention[31]. Stage II bladder cancer (T2) (**FIG. 4**) is the first muscle-invasive stage of the disease, characterized by tumour penetration into the detrusor muscle[18]. This level of infiltration represents a critical prognostic threshold, as the transition from non-muscle-invasive to muscle-invasive disease is associated with a marked decrease in patient survival[32], due to the significantly increased risk of systemic dissemination[33]. Whereas T2 bladder cancer is confined to the detrusor muscle layers, further local tumour extension may result in invasion beyond the bladder wall into the perivesical soft tissue, most commonly the perivesical fat. Such an infiltration constitutes stage III (T3) urinary bladder cancer (**FIG. 4**) and indicates a more advanced extent of local tumour spread[18]. It is further classified as stage IIIA, characterized by microscopic invasion of the perivesical soft tissue, and as stage IIIB, when extravesical infiltration is macroscopically evident[34]. Beyond stage III disease, continued local tumour invasion may lead to direct invasion of adjacent organs and structures, marking the transition to Stage IV (T4) bladder cancer[18] (**FIG. 4**). T4 disease

is subdivided into stage IVA, when the tumour invades the prostatic stroma, uterus, or vagina, and stage IVB, in which the tumour extends into the pelvic wall or abdominal wall[34]. In addition to the local tumour extent defined by T category, ranging from T1 to T4 stages, the TNM staging system provides a standardized method for the classification of regional lymph node involvement and distant metastatic spread[18]. Regional lymph node status is categorised as: Nx, in which regional lymph nodes cannot be assessed; N0, indicating no regional lymph node metastasis; N1, defined by a single regional lymph node metastasis in the lesser pelvis; N2, characterized by multiple regional lymph node metastases in the lesser pelvis; and N3, indicating lymph node metastasis to the common iliac lymph nodes[18]. Metastatic involvement of lymph nodes beyond the common iliac chain is considered distant metastatic disease[35]. Distant metastases are further subdivided into M1a, representing metastases limited to non-regional lymph nodes beyond the common iliac nodes, and M1b, defined by metastases to distant organs or non-lymph node sites[18].

3. Immune system and tumour microenvironment definition

3.1 Immune system

The immune system evolved to protect multicellular organisms from pathogens. Highly adaptable, it defends the body against invaders of any kind, being able to distinguish the infectious non-self from the non-infectious self. This diversity of potential pathogens requires a range of recognition and destruction mechanisms to match the multitude of invaders[36]. To accomplish this feat, vertebrates have evolved a complicated and dynamic network of cells, molecules, and pathways[36]. Although reference is made to "the immune system," it is important to appreciate that immunity was artificially divided into two interconnected systems: innate and adaptive. Innate immunity includes built-in molecular and cellular mechanisms that are encoded in the germline and are evolutionarily more primitive, aimed at preventing infection or quickly eliminating common invaders[36]. This includes physical and chemical barriers to infection, and also a series of preexisting serum proteins, collectively referred to as complement, that bind common pathogen-associated structures and initiate a cascade of labeling and destruction events[36]. This first line of defense prevents most pathogens from taking hold or eliminates infectious agents within hours of encounter. The recognition elements of the innate immune system, though, are

not very specific and are therefore unable to distinguish between small differences in foreign antigens. A second form of immunity, known as adaptive immunity, is much more attuned to subtle molecular differences. It evolves in real time in response to infection and adapts to better recognize, eliminate, and remember the invading pathogen. This part of the system, which relies on B and T lymphocytes, takes longer to come on board but is much more antigen-specific. Typically, it takes 5 or 6 days after initial exposure before an adaptive immune response[36]. After antigen encounter, T and B lymphocytes undergo selection and proliferation[36]. Although slow to act, once B and T cells have been selected, they can typically resolve the infection.

3.2 Tumour microenvironment

From an immunologic perspective, cancer cells can be viewed as altered self cells that have escaped normal growth-regulating mechanisms[36]. For this reason, most of the antigens associated with them are recognized as self and subject to tolerance. However, unique or inappropriately expressed antigens can be found in many tumours and are frequently detected by the immune system, which may help safeguard homeostasis by rejecting tumoral cells. Although several key immune cell types and effector molecules that participate in this response have been identified in recent years, much still remains to be learned about mechanisms of anti-tumour immunity and how to induce these in clinical settings[36]. The process of immune recognition of tumours is not unidirectional, and it has been formalised as cancer immunoediting, comprising three phases: elimination, in which transformed cells are destroyed by a competent immune system; equilibrium, in which the surviving tumour cells persist under immune pressure and are progressively sculpted; and escape, in which immunologically edited tumours grow progressively, become clinically apparent and establish an immunosuppressive microenvironment[37]. The setting in which this interaction takes place is the tumour microenvironment (TME). Tumours are increasingly regarded as complex ecosystems comprising cancer cells together with a multitude of non-malignant cells (immune cells, cancer-associated fibroblasts, endothelial cells and pericytes) embedded in an altered extracellular matrix. These host cells, once considered bystanders of tumorigenesis, are now known to play critical roles in cancer pathogenesis, and both the composition and the functional state of the TME vary extensively with the organ of origin, the tumour

stage and the individual patient[38]. In parallel, the physical and chemical conditions that develop within a growing tumour, most notably hypoxia, resulting from rapid proliferation outpacing vascular supply, together with acidosis, competition for nutrients and increased tissue stiffness, further impair the function of infiltrating lymphocytes while favouring tumour cell adaptation[38].

4. Bladder tumour microenvironment

4.1 Stromal-vascular interface

The bladder tumour microenvironment is a complex system in which malignant urothelial cells co-opt non-malignant elements to promote tumour growth and survival[39]. It comprises non-malignant cellular components, including stromal cells, immune cells, and vascular elements, as well as non-cellular components such as extracellular matrix (ECM)[39]. In addition, the tumour microenvironment encompasses various physical and chemical conditions, including hypoxia, tissue stiffness, and oxidative stress, which influence tumour development and progression[39]. A major component of the tumour microenvironment (TME) is represented by cancer-associated fibroblasts (CAFs)[40], which are activated or reactive fibroblasts[41] that mainly originate from tissue-resident fibroblasts or pericytes[42] and surround cancer cells. They are stimulated by biochemical signals from urothelial cancer cells, such as TGFβ1[43] and PDGF[44], by oxidative stress[45], and by inflammatory cytokines, such as IL-1 from immune or urothelial cells[46]. In pathological conditions, CAFs are continuously activated, altering biological functions and increasing tissue stiffness as a mechanism to exert pro-tumorigenic roles[47]. This contrasts with healthy tissues, where fibroblasts are typically quiescent and become transiently activated during wound healing to support tissue repair[48]. In the context of bladder cancer, it is possible to distinguish between two different CAF subtypes, which are RGS5+ αSMA-high myofibroblasts (myCAFs) and IL-6+, PDGFRαhigh inflammatory fibroblasts (iCAFs)[49] (**FIG. 5**). CAFs promote bladder cancer progression by secreting chemoattractants, including CC-chemokine ligand 5 (CCL5)[50] and connective tissue growth factor (CTGF)[51]; growth factors, such as basic fibroblast growth factor 2 (FGF2)[51]; angiogenic factors, including vascular endothelial growth factor (VEGF)[52] and platelet-derived growth factor (PDGF)[52]; and ECM-remodelling metalloproteinases (MMPs)[53] (**FIG. 5**). Beyond affecting cancer cells, CAFs shape the immune environment by producing transforming growth factor-β1 (TGFβ1), which

suppresses immune response and is associated with a T cell exclusion phenotype in human bladder cancer[54].

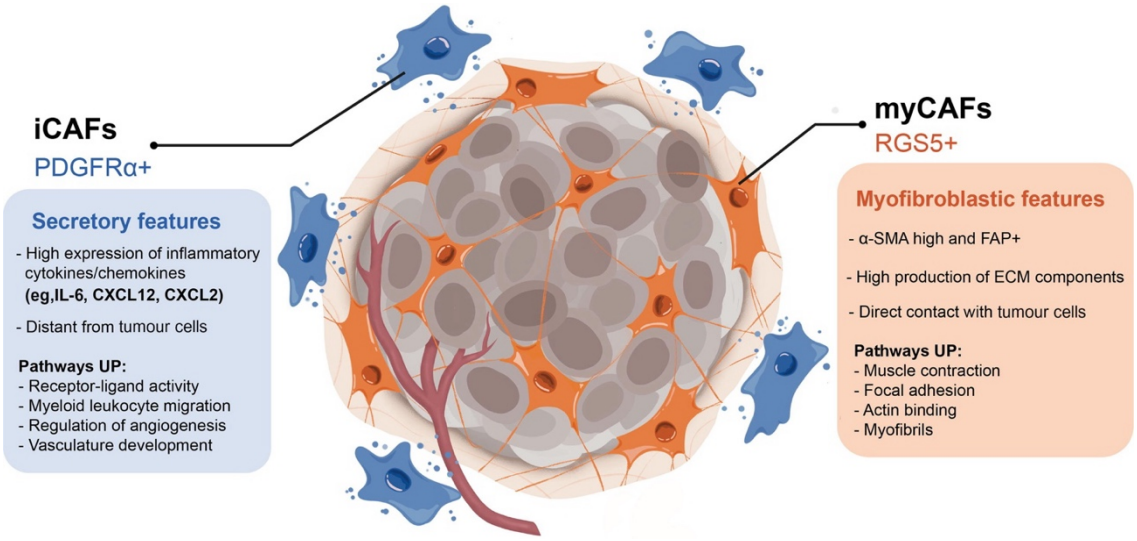

***FIG. 5*. Cancer-associated fibroblasts in bladder cancer.** CAFs in bladder cancer are divided into myCAFs, and iCAFs. myCAFs restructure the scaffolding of the tissues surrounding cancer cells by producing ECM components and pulling them together via muscle contraction. iCAFs are more distant from tumour cells, and their principal role is to establish chronic inflammation, leading to an immunosuppressive environment, and to regulate angiogenesis to nourish the tumour cells. *Caramelo et al., 2023*

Besides CAFs, the vasculature system represents another key structural component of the TME. In a healthy bladder, the urothelium, the lamina propria, and the detrusor muscle are supplied by an organized microvasculature network of endothelial cells supported by a basement membrane and surrounded by pericytes[55] (**FIG. 6**). In contrast, tumour-associated vasculature is highly altered[56]. Although tumour blood vessels still comprise endothelial cells and pericytes, the endothelial cells are often immature and exhibit reduced pericyte coverage, weakened intercellular junctions, and structural instability[57] (**FIG. 6**). As a result, these vessels are frequently collapsed, tortuous, and hyperpermeable, contributing to impaired perfusion, hypoxia, and tumour progression[57]. Moreover, bladder cancer cells secrete vascular endothelial growth factors (VEGFs), which stimulate endothelial cells to release von Willebrand Factor (VWF), a factor known to induce platelet aggregation and subsequent blood vessel occlusions, which have also been associated with poor patient outcomes in bladder cancer[58].

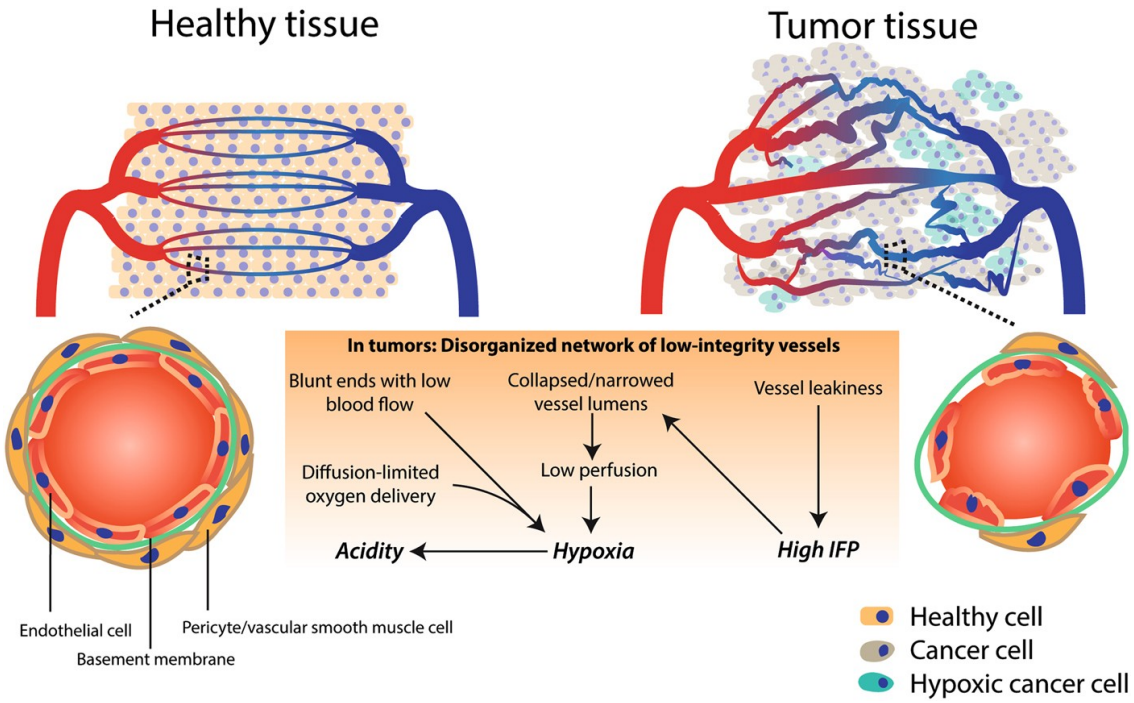

***FIG. 6*. Vasculature system organization in healthy and tumour tissue.** In healthy tissue, blood vessels are well ordered and space through each other so that they can perfuse all corners. They also display the correct structure of endothelial cells surrounded and supported by a basement membrane, which is further enclosed in pericytes. In tumour tissue, the vasculature system loses its organization, and vessels are structurally unstable, leading to leakiness.This phenomenon increases interstitial fluid pressure (IFP), with subsequent collapse of vessel lumens, low perfusion, and hypoxia. Tumoral cells in hypoxic conditions enhance glycolysis, leading to acidification of the pH of the TME, which has been associated with recruitment of immunosuppressive immune cells, reduced cytotoxic activity of effector T cells, and hampered delivery of chemotherapeutic or immunotherapeutic drugs (Chouaib et al., 2016). *Schaaf et al., 2018*

4.2 Tumour-infiltrating lymphocytes

The immune landscape of bladder cancer is largely defined by the spatial distribution and density of tumour-infiltrating lymphocytes (TILs), which constitute a central component of the host immune response within the bladder tumour microenvironment (TME) and reflect the immune system's capacity to recognize and eliminate malignant cells[59]. The abundance and localization of these lymphocytes within the tumour and surrounding stroma enable the classification of tumours into three distinct immune phenotypes: T-cell inflamed, immune-excluded, and immune-desert[60]. These phenotypes are associated with differences in antitumour immunity, disease progression and response to immunotherapy[60]. In particular, "T-cell inflamed" or "hot" tumours are characterized by high levels of TILs within the tumour bulk (**FIG. 7**), which generally correlate with a

more favourable prognosis and better response to therapies[60]. In contrast, the immune-excluded phenotype reports TILs accumulation within the surrounding stromal compartment, where they are prevented from penetrating the tumour parenchyma[60] (**FIG. 7**). Physical barriers, such as dense extracellular matrix enriched with collagen and fibronectin, together with stromal-mediated immunosuppressive signals, restrict T-cell infiltration and limit their ability to eliminate malignant urothelial cells. “Immune-desert” or "cold" tumours display a profound lack of TILs, indicating a complete failure in immune recruitment or recognition[60] (**FIG. 7**).

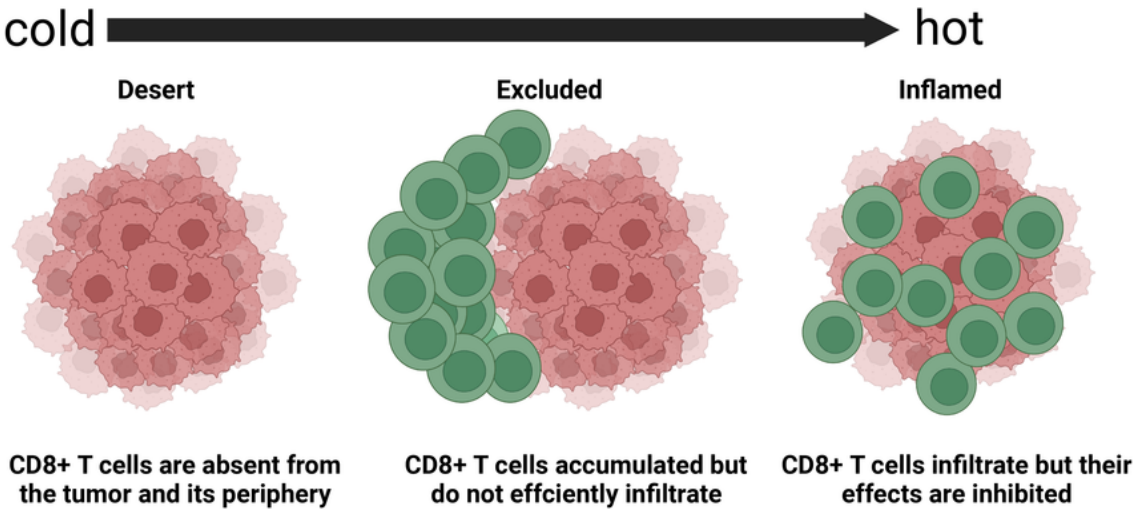

FIG. 7. **Classification of tumours based on the infiltrating lymphocytes.** In immune-desert tumours, CD8+ T cells are absent from the tumoral site and also from the periphery, indicating a lack of recruitment or recognition of the cancer cells. In immune-excluded tumours, CD8+ T cells are recruited, but they cannot infiltrate within the tumour because of physical barriers. In immune-hot tumours, CD8+ T cells effectively infiltrate the tumour, although their cytotoxic activity is often inhibited. *Wu et al., 2023*

Throughout the tumour microenvironment, cytotoxic CD8+ T cells act as the primary antitumor effectors by recognizing foreign antigens and inducing cytotoxin-mediated tumour cell death through the release of perforin and granzymes[61]. A high density of CD8+ T cells is a strong predictor of overall survival, but their efficacy is often neutralized by immunosuppressive populations, including regulatory T cells (Tregs) and myeloid-derived suppressor cells (MDSCs)[62]. Moreover, recent discoveries pinpoint B cells as active participants in the bladder TME, demonstrating the ability to orchestrate the immune response[63]. They may play either an antitumoral role or a pro-tumoral, immunosuppressive role according to their phenotype and spatial organization[63]. In

healthy tissues, B cells contribute to antitumor immunity through multiple mechanisms. As professional antigen-presenting cells (APCs), they capture tumour-derived antigens and present them to CD4+ T cells, promoting their activation[64]. In addition, mature B cells and plasma cells secrete tumour-specific antibodies that can engage Fcγ receptors on natural killer cells or macrophages, triggering antibody-dependent cellular cytotoxicity and phagocytosis of cancer cells[63,65]. Certain effector B cell subsets can also directly attack cancer cells by releasing granzyme B, which induces caspase-mediated apoptosis, and releasing tumour necrosis factor-related apoptosis-inducing ligands (TRAIL), which bind death receptors on target cells, triggering apoptosis[66]. It has been highlighted how B cells are also a fundamental component of tertiary lymphoid structures (TLS), which are organized aggregates of immune cells that form postnatally in non-lymphoid tissues during chronic inflammation or malignancy[67]. TLSs anatomically resemble secondary lymphoid organs, typically featuring a T cell zone and a B cell zone, supported by specialized high endothelial venules[67]. The proximity of TLS to the tumour allows local priming of T and B cells with tumour-specific antigens, bypassing the lymph nodes[67]. Furthermore, TLSs allow B cell clonal expansion, somatic hypermutation, and isotype switching, plus CD8+ T cell activation[68]. TLS presence has been associated with an improvement in overall survival and increased response to immunotherapy in many different tumour types[69]. However, some studies correlate the presence of TLS with tumour progression[70]. A variety of immunosuppressive mechanisms have been proposed to account for this phenomenon. In a murine lung adenocarcinoma model, Tregs were found to be predominantly localized within TLSs, making them immune suppressive aggregates rather than promoting their potential as antitumorals[71]. Moreover, it has been shown that TLS-resident B cells may secrete IL-10, which exerts an immunosuppressive role[67]. In summary, tertiary lymphoid structures are well- organized immune aggregates whose prognostic impact remains context-dependent and varies across different cancer types[67]. Nevertheless, recent literature points out that manipulating TLS formation and cell composition represents a promising strategy for the development of immunotherapy[72]. Another way B cells can negatively contribute to immune response and patient outcome is through an immunosuppressive subset, named Bregs, which is normally needed to keep the immune response in check[73]. In the cancer context, though, Bregs can be induced by CAFs, and they can support tumour progression by secreting

inhibitory cytokines, including IL-10, IL-35, and TGFβ[74]. Moreover, IgA+ isotype-switched B cells in the peritumoral or intratumoral spaces have been associated with an immunosuppressive environment[75], and in bladder cancer, high IgA expression from B cells is correlated with shorter overall survival in patients treated with immunotherapy[76]. Beyond these general mechanisms, recent work has begun to resolve the B cell compartment of bladder cancer specifically at the level of individual subsets, revealing a picture in which the balance between B cell states, rather than their overall abundance, appears to determine the outcome. Single-cell profiling of muscle-invasive tumours has identified naive, proliferating, interferon-stimulated and germinal centre-associated B cells alongside plasma cells and has shown that the interferon-stimulated and germinal centre-associated subtypes are specifically enriched in MIBC, where their infiltration, together with the presence of TLS, correlates with a more favourable prognosis[77]. The role of the plasma cell compartment appears to be similarly context-dependent, with the isotype of the antibody response emerging as a more informative parameter than plasma cell abundance alone. In bladder cancer, a high intratumoral IgG1/IgA ratio has been shown to be associated with a higher cytotoxic gene signature, T cell receptor signaling, and improved response to anti-PD-L1 therapy[78]. Despite these advances, the mechanisms governing B cell behaviour across the different stages of bladder cancer remain largely undefined, and the role of B cells in non-muscle-invasive disease is considerably less characterised than in muscle-invasive tumours.

4.3 Other immune cells

The tumour microenvironment is not exclusively composed of lymphocytes, but includes several other immune cell types that greatly influence patient outcome[79]. Recent single-cell analyses have identified one specialized dendritic cell subgroup, LAMP3+ DCs, which actively recruit Tregs to the tumour site by secreting the cytokines CCL17, CCL19, and CCL22, all of which exhibit strong chemotactic activity toward Tregs via binding to CCR4 on their surface[80]. Besides dendritic cells, macrophages have been recognized for their pro-tumorigenic activity. In fact, the ones residing within the tumour or recruited from the bone marrow into hypoxic and necrotic intratumoral areas can differentiate into tumour-associated macrophages (TAMs)[81]. TAMs enhance cancer progression, including tumour growth, metastatic spread, and resistance to therapy, by secreting growth factors,

cytokines, and proteases[82]. They also sustain chronic inflammation, which suppresses effective antitumour immune responses, by releasing mediators such as tumour necrosis factor (TNF), TGFβ, IL-6, and IL-12[82]. Although macrophages can adopt a broad spectrum of activation states, they are commonly classified into pro-inflammatory M1-like and pro-tumoral M2-like subsets[83]. M1-like macrophages promote acute inflammatory responses against pathogens and tumour cells, whereas M2-like macrophages drive chronic inflammation, leading to immunosuppression and supporting tumour growth[83]. In bladder cancer, TAMs are predominantly pro-tumoral M2-like and highly present in high-grade tumours compared to low-grade lesions[82]. Understanding the balance within the immune compartment is critical for clinical management, as the ratio of effector CD8+ T cells to immunosuppressive populations such as myeloid-derived suppressor cells (MDSCs) or regulatory T cells (Tregs) serves as a crucial predictor of responses to neoadjuvant chemotherapy and modern immunotherapies[84]. Ultimately, the transition of a tumour from an immune-excluded to a T-cell-inflamed state remains a primary goal for enhancing the effectiveness of existing treatments and developing new therapeutic strategies[85].

5. Main lines of therapy for bladder cancer

5.1 Non-muscle invasive bladder cancer

The management of bladder cancer is highly dependent on the stage and grade, moving from localized intravesical treatments to systemic therapies as the disease advances[19,20]. Since, by definition, NMIBC is confined to the urothelium or lamina propria, the cornerstone of treatment is transurethral resection of bladder tumour (TURBT). In general, TURBT is a diagnostic, staging, and therapeutic tool consisting of a first comprehensive inspection of the bladder, followed by resection of the tumour, the underlying bladder wall, and the surrounding area[20]. In NMIBC, TURBT alone can provide complete resection of the lesion[86]. Nonetheless, low-grade Ta/T1 tumours commonly recur and may progress to MIBC[87]. Therefore, to minimize the risk of relapse, a single, immediate, postoperative intravesical instillation of chemotherapeutic agents is recommended [86]. High-grade Ta/T1 lesions and all CIS lesions require the combination of TURBT with intravesical instillations of Bacillus Calmette-Guérin (BCG), which is a live attenuated strain of *Mycobacterium bovis*, which was proposed in 1976 as an adjuvant

immunotherapy to treat bladder cancer[88], beyond being developed as a tuberculosis vaccine[89], and is now the gold standard for treatment of high-grade NMIBC[90]. Its mechanism of action is not yet fully understood, but BCG is known to induce a localized non-specific immunological response that leads to recruitment of immune cells and release of cytokines, which, as a secondary effect, lead to tumour eradication[91]. The standard of care is one BCG instillation per week for 6 weeks after TURBT to stimulate the immune response, followed by a maintenance phase of BCG at 3, 6, 12, 18, 24, 30, and 36 months after induction[92]. BCG intravesical treatment has more side effects than intravesical chemotherapy, but serious adverse events are encountered in 5% of patients and can be treated effectively[93], while BCG immunotherapy has shown greater survival rates compared to chemotherapy[90]. Some NMIBC patients may relapse or become not sensitive to BCG immunotherapy after an initial response, or not respond at all[94]. For these patients, the standard option is radical cystectomy, a surgical procedure in which the entire urinary bladder, nearby lymph nodes, and adjacent organs (prostate and seminal vesicles for men, uterus, ovaries, fallopian tubes for women) are removed[19].

5.2 Muscle-invasive bladder cancer (MIBC) and metastatic bladder cancer

Muscle-invasive bladder cancer (MIBC) requires invasive local treatment combined with systemic therapy to reduce the high risk of recurrence and metastasis[19]. Therapy commonly consists of cisplatin-based neoadjuvant chemotherapy (NAC) followed by radical cystectomy[19]. For patients unfit for surgery or cisplatin-based chemotherapy, as well as for selected patients who prefer to avoid surgery, trimodality therapy (TMT), consisting of maximal TURBT followed by radiosensitization and radiotherapy, is an accepted treatment alternative[19]. Patients at high risk of recurrence after surgery may undergo adjuvant therapy with the immune checkpoint inhibitor (ICI) nivolumab, an anti-PD1 monoclonal antibody[95]. However, after progression to metastatic disease, treatment shifts to a systemic approach focused on prolonging survival and maintaining quality of life[19]. The standard first-line management for metastatic disease is cisplatin-based combination chemotherapy, specifically composed of methotrexate, vinblastine, adriamycin, and cisplatin (abbreviated as MVAC), followed by maintenance avelumab

ICI therapy[19]. Patients who are cisplatin ineligible due to age or comorbidities can either receive gemcitabine plus carboplatin or ICIs targeting PD-1 and PD-L1[19].

5.3 Immunotherapy in bladder cancer

Bladder cancer has historically been one of the most receptive tumour types to immunotherapeutic intervention, and intravesical BCG, described above, remains the earliest and longest-standing example of a successful cancer immunotherapy. Over the past decade, the therapeutic repertoire has expanded considerably, with drugs now approved across all disease stages and acting through distinct immunological mechanisms. The largest class comprises the immune checkpoint inhibitors, monoclonal antibodies directed against the PD-1 receptor or its ligand PD-L1. Tumour cells and infiltrating immune cells frequently express PD-L1, which engages PD-1 on T lymphocytes and delivers an inhibitory signal that restrains effector function[96]. By blocking this interaction, these agents release the brake on pre-existing antitumour T cell responses[97]. For patients with high-risk NMIBC who are unresponsive to BCG, three agents have been approved since 2020, all indicated for carcinoma in situ with or without papillary tumours[20]. Pembrolizumab, an anti-PD-1 antibody, was the first, approved in 2020. Nadofaragene firadenovec, approved in December 2022, was the first gene therapy developed for bladder cancer: it is a non-replicating recombinant adenoviral vector that delivers the human interferon-α2b gene into urothelial and tumour cells, which are thereby induced to express the cytokine locally, producing immunostimulatory, antiangiogenic and pro-apoptotic effects[98]. Nogapendekin alfa inbakicept, approved in April 2024 in combination with BCG, is an IL-15 superagonist consisting of an IL-15/IL-15Rα-Sushi-Fc fusion complex that promotes the activation and proliferation of $CD4^+$ and $CD8^+$ T cells, NK cells and memory T cells, acting synergistically with the innate stimulation provided by BCG[99]. More recently, immunotherapy has been extended to patients who have not yet received BCG: durvalumab, an anti-PD-L1 antibody, was approved by the FDA in 2026 in combination with BCG for BCG-naive high-risk NMIBC following TURBT[100]. Regarding MIBC, Adjuvant nivolumab, an anti-PD-1 antibody, was approved for high-risk muscle-invasive urothelial carcinoma after resection[101]. The combination of pembrolizumab with the antibody-drug conjugate enfortumab vedotin,

which targets Nectin-4, widely expressed on urothelial carcinoma, has been approved by the FDA as neoadjuvant treatment followed by adjuvant treatment after cystectomy for all patients with MIBC who are candidates for surgery, extending an earlier approval restricted to cisplatin-ineligible patients[102]. A further development is the introduction of molecularly guided treatment selection: atezolizumab was approved in 2026 as adjuvant therapy specifically for patients with detectable circulating tumour DNA molecular residual disease after cystectomy, identified by a companion diagnostic test, so that only patients with evidence of residual disease are exposed to treatment and its associated toxicity[103]. Despite this expansion of the therapeutic repertoire, several limitations remain. Responses to checkpoint inhibition are highly variable: only a subset of patients derive durable benefit, while many experience primary or early resistance[104]. Even in the settings where immunotherapy has been most impactful, absolute response rates remain less than half. In BCG-unresponsive NMIBC, for instance, only 41% of patients treated with pembrolizumab achieved a complete response at three months[105], and for those who do not respond, radical cystectomy remains the fallback option.

5.4 Limitations of current therapies and unmet clinical needs

Beyond the choice of therapy, however, a more fundamental clinical problem precedes it. Approximately 75% of bladder cancers are non-muscle-invasive at diagnosis, and of these, 10-20% will progress to muscle-invasive disease[106]. This transition is the single event that most decisively determines a patient's prognosis: once muscle invasion has occurred, the risk of distant metastasis increases substantially and management shifts from conservative transurethral resection to radical cystectomy or systemic therapy, with the associated morbidity and impact on quality of life[107]. Crucially, patients at high risk of progression derive benefit from early cystectomy performed before invasion occurs[19], which means that the ability to identify them in advance would translate directly into a change in management rather than merely into refined prognostic information. The contrary is equally important: radical cystectomy is a major and irreversible intervention, and some patients who would not have progressed mistakenly undergo it[19]. It has been estimated that current risk stratification fails to correctly predict the transition to muscle-invasive disease in approximately 30% of cases[107]. Molecular markers capable of refining

the current models are therefore needed. In this context, the immune compartment is a strong candidate. The immune system has a key role in determining bladder cancer course, as demonstrated by the efficacy of BCG, and the tumour immune microenvironment actively changes as the disease evolves, making it a potential source of distinct features that precede transition to MIBC.

AIM OF THE STUDY

The following study was carried out in the Tumour Microenvironment Unit at Humanitas University. The working hypothesis of this project was that the immune microenvironment of bladder cancer differs between tumours at different stages of progression, and that differences reflect processes that accompany, and possibly contribute to, the acquisition of an invasive phenotype. Identifying such features could therefore serve a dual purpose: refining our understanding of how the disease evolves, and revealing specificities that might be exploited either as prognostic markers of progression or as therapeutic targets. On this basis, my thesis work aimed to provide a high-resolution characterisation of the immune profile of bladder cancer patients, focusing on the transcriptomic shifts occurring across the transition between non-muscle-invasive and muscle-invasive disease. To this end, single-cell RNA sequencing was performed on tumour tissue from a cohort of bladder cancer patients. Central to this analysis were the reclusterings of the major immune populations, which allowed a higher resolution examination of the differences between immune subsets than the initial clustering permitted, and which directed the subsequent work towards the B cell compartment. The second aim was to determine whether the alterations observed in patients could be reproduced experimentally and attributed to tumour-derived secreted factors. The impact of the bladder cancer secretome was therefore evaluated through controlled *in vitro* experiments, in which splenic B cells were exposed to conditioned medium from a murine bladder cancer cell line, both under resting conditions and in the presence of stimuli driving differentiation into plasma cells, in order to establish how tumour-derived factors influence B cell maturation and differentiation. Finally, a carcinogen-induced mouse model was generated to reproduce spontaneous tumour development within an intact organism, allowing the immune compartment to be compared between early and late stages of disease to test whether the phenotypes identified in patients and *in vitro* were also detectable in a physiological setting.

MATERIALS AND METHODS

Cell culture

The MB49 cell line was purchased from Sigma-Aldrich. The cells were grown in RPMI 1640 without L-glutamine (Euroclone) supplemented with 10% heat-inactivated FBS (Sigma-Aldrich), penicillin/streptomycin solution (penicillin G 10U/ml + streptomycin 0.1mg/ml; Euroclone), 2,5mM L-glutamine (Euroclone) at 37°C in 5% CO2. For conditioned medium production, $2x10^5$ MB49 cells were seeded in T75 flasks and cultured for 72 hours in supplemented RPMI medium: conditioned medium was then harvested, centrifuged to pull down remaining cells, and the supernatant collected and stored at -80°C. B cells were obtained from the spleens of C57CL/6 male mice. The spleens were smashed on a 100 μm-diameter filter (FALCON) using the knurled part of the piston of a 1 mL FARMATEXA Softouch syringe (MED'S MEDICAL SOLUTIONS), and single cells were harvested in a 50 mL FALCON tube. The filter was washed with supplemented RPMI medium for maximum yield. The cells were pulled down by centrifugation, and the supernatant was removed. Cells were subsequently resuspended in 1 mL ACK Lysis Buffer (Gibco) for each spleen for red blood cell lysis for 10 minutes at 4°C. The FALCON tube was then topped up to 50 mL with supplemented RPMI medium, centrifuged to pull down the cells, and the supernatant was discarded. Cells were then resuspended in MACS buffer, prepared with PBS supplemented with 10% BSA, and Biotin-Antibody Cocktail, mouse (Miltenyi) was added. After 5 minutes of incubation at 4°C, additional MACS buffer and the Anti-Biotin MicroBeads (Miltenyi) were added, and the sample was incubated for 10 minutes at 4°C. Magnetic separation of untouched resting B cells was then performed through negative selection with an MS column (Miltenyi) on a MiniMACS separator (Miltenyi). Then, $2x10^5$ per well of the separated B cells were seeded in 96-well round-bottom cell culture plates in supplemented RPMI with the addition of BAFF (R&D Biosystems) 50 ng/mL, IL-7 (Peprotech) 20 ng/mL, and β-mercaptoethanol (Gibco) 50 μM.

Mice

All mice were maintained under specific pathogen-free conditions of the Humanitas Clinical and Research Institute, and experiments were performed according to national guidelines approved by the Italian Health Ministry. C57BL/6 mice were provided by Charles River. For induction of spontaneous bladder tumours, random mice were given N-Butyl-N-(4-hydroxybutyl)nitrosamine (BBN) diluted at 0,05% in tap water for 12 weeks, while the other ones were given regular tap water and kept as a control. The BBN solution was then substituted with regular tap water, and tumour growth was monitored every other day by measuring tumour size with a caliper. Mice were sacrificed 4 weeks and 12 weeks after the end of the treatment.

Flow cytometry

For the conditioned medium B cell experiment, B cells were treated with Brefedin A (Bio-Legend) 5 μg/mL 68 h after plating to inhibit protein secretion. After 4 h, they were stained with LIVE/DEAD Fixable Viability Dye eFluor 780; Bio-Legend) 10 min at RT, followed by staining with the following antibody mix: CD27-PECy7, CD11b-PE-CF594, CD19-PerCPCy5.5, CD25-RB780, CD138-BV510, CD23-BV650, CD22.2-BUV805, LAP-APC, IgD-BUV496, CD21/CD35-BV421, CXCR4-BV605, NK1.1-BUV395, CD45-BUV563, IgM-BUV615, CD3-BUV661, CD274-BV786, CD5-BUV737, CD44-AF700, CD20-Pecy5 (BD Biosciences and BioLegend) for 20 min at room temperature. For AREG and IL-10 detection, after extracellular staining, samples were fixed and permeabilized (Foxp3 / Transcription Factor Staining Buffer Set; eBioscience) and stained with AREG-AF488 and IL-10-PE antibodies. Each antibody was previously titrated to identify the optimal working dilution. Cells were then fixed in 0,05% PFA and acquired using the BD FACSymphony system. For the BBN bladder cancer induction experiment, tumour samples were processed for single-cell suspensions. Briefly, tumours were mechanically dissociated into a solution with 1mg/ml collagenase V (Gibco BRL, Thermo Fisher Scientific) in RPMI 1640 on a rocking platform at 37°C in 5% CO2 for 20 min. The cell suspension was then centrifuged and digested for an additional 5 min with 2.5% trypsin (Gibco BRL, Thermo Fisher Scientific), which was then inactivated by adding complete medium with FBS. The cell suspension was then passed through a syringe needle several times until dissociated and filtered through a 40μm cell strainer.

Cell suspension was then incubated with Fc block. Cells were stained with LIVE/DEAD Fixable Viability Dye eFluor 780; Bio-Legend) 10 min at RT, followed by staining with the following antibody mix: MHCII-BV480, Ly6G-BV570, CD27-PECy7, CD45-BUV563, CD23-BV650, CD4-BV711, CD25-AF488, F480-APCH7, NK1.1-BUV395, IgD-BUV496, CD8-BUV805, CD21/CD35-BV421, CXCR4-BV605, CD11b-PECF594, CD19-PerCPCy5.5, IgM-BUV615, CD138-BV750, CD3-BUV661, CD44-AF700, CD5-BUV737, CD274-BV786, CD20-Pecy5 (BD Biosciences and BioLegend) for 20 min at room temperature. For TGFβ and IL-10 detection, after extracellular staining, samples were fixed and permeabilized (Foxp3 / Transcription Factor Staining Buffer Set; eBioscience) and stained with TGFβ-APC and IL-10-PE antibodies. Each antibody was previously titrated to identify the optimal working dilution. Cells were then fixed in 0,05% PFA and acquired using the BD FACSymphony system. For the sorting experiment, cells were stained for CD45, EpCAM, and viability dye. CD45+EpCAM- and CD45-EpCAM+ cells were sorted using BD FACSAria III.

Single-cell RNA sequencing

Sorted CD45+EpCAM- cells and CD45- EpCAM+ cells were loaded into one channel of the Single Cell Chip A using the Single Cell 39 v2 Reagent Kit (10X Genomics) for generation of gel bead emulsion into the Chromium system. Following capture and lysis, cDNA was synthesized and amplified for 14 cycles according to the manufacturer's protocol (10X Genomics). 50 ng of the amplified cDNA was then used for each sample to construct Illumina sequencing libraries. Sequencing was performed on the Illumina NextSeq 500 sequencing platform following 10X Genomics instruction for reads generation. A sequencing depth of at least 20,000 reads/cell was obtained for each sample. Raw sequencing data in the format of BCL files were converted into FASTQ files and aligned to the human reference genome GRCh38, taking advantage of the Cell Ranger Pipeline (version 593.0.2) provided by 10X Genomics. We used the findIntegrationAnchors function using 2,000 anchor genes to integrate all four samples and combine datasets. After integration, a subgroup of 5232 cells from Days 14 and 21 was selected, and a quality check was performed. Cells with a precise feature count range of 200–2500 (nfeatures) were analysed by applying Principal Component Analysis (PCA) on the combined dataset. We selected the first 30 major components to perform Louvain

clustering and Uniform Manifold Approximation and Projection (UMAP) embedding at a resolution of 0.3. Analysis resulted in a landscape that includes 15 different clusters. Then we processed each individual dataset separately, choosing the top 2,000 most variable genes for each dataset, using Seurat R package (versions 3.0.2 and 3.5.1 of R; Stuart et al., 2019). The final analysis produced 15 clusters, identified from the original individual datasets as well as the integrated subset. To assign clusters to cell types, we used Single Cell Expression Atlas as the reference dataset.

Statistical analyses

Statistical analyses were performed using two-tailed unpaired or paired Student's t test and one-way ANOVA as specified. Pearson's test was used for the correlation analyses. Values are presented as mean ± SEM (*, $P < 0.05$; **, $P < 0.01$; ***, $P < 0.001$; **** $P < 0.0001$). Data were analysed using Rstudio 2026.05.0+218 software.

RESULTS

1. Single-cell RNA sequencing of bladder cancer patients

1.1 Experimental plan and merged analysis

Given the major involvement of the immune system in bladder cancer progression[51,60,108,109], we characterised the immune profile of bladder cancer patients, tracing the main differences between NMIBC and MIBC tumours. To do so, we adopted single-cell RNA sequencing (scRNA-seq) technology to evaluate the distribution and transcriptional profiles of immune cells in muscle-invasive and non-muscle-invasive bladder cancer (**FIG. 8**). In particular, we enrolled a cohort of 73 bladder cancer patients who underwent either TURBT or cystectomy, depending on their individual tumour stage and grade. From this initial cohort, 19 patients were selected for scRNA-seq analysis, including 9 NMIBC tumours, 8 MIBC tumours, and 2 benign papilloma tissues. We stained the tissues for epithelial and immune lineage markers and performed cell sorting with a fluorescence-activated cell sorter (FACS) to enrich the cellular suspensions to 90% immune and 10% epithelial cells (**FIG. 8**). This step was essential to make sure that the subsequent scRNA-seq would highlight the shifts in immune populations across different bladder cancer stages, rather than shifts in the tumoral compartment. Sequencing of the single-cell suspensions generated raw data on their transcriptional profiles, which required rigorous quality-control pipelines to remove common technical artifacts and low-quality sequencing events, ensuring that the remaining dataset accurately reflects the diverse cellular landscape. Following this quality control, we performed unsupervised clustering to delineate distinct cell populations based on their unique transcriptional signatures (**FIG. 8**).

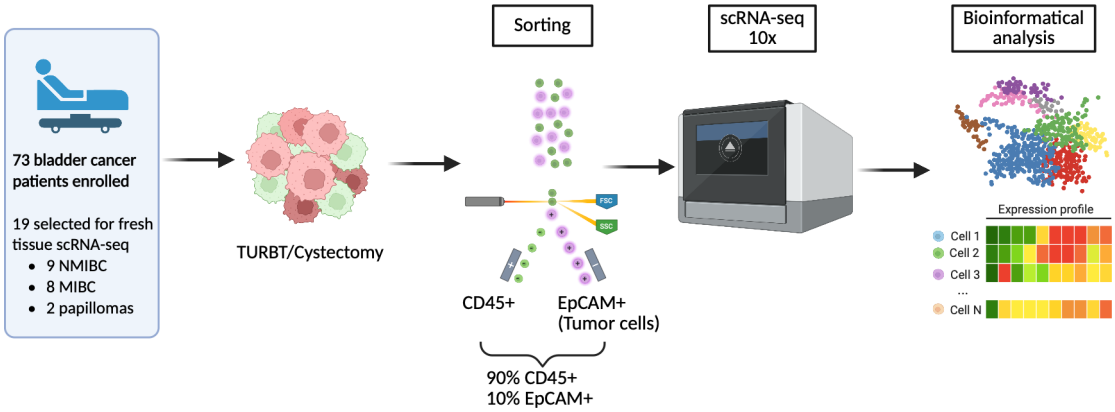

***FIG. 8*. Experimental scheme for the profiling of the immune microenvironment by scRNA-seq in the bladder of NMIBC patients and MIBC patients.** The study started with the enrollment of 73 patients, of whom 24 underwent radical cystectomy, and 49 underwent TURBT. 11 of them were categorized as screening failures, meaning the biopsy was considered non-tumoral. After tumour dissociation and cell number assessment, only 9 NMIBC tumours, 8 MIBC tumours, and 2 non-tumour tissues were sufficient to proceed with cell sorting and scRNA-seq. The selected samples were then stained with an antibody specific for CD45, the leukocyte common antigen, and one specific for EpCAM, the lineage marker of epithelial cells. Both antibodies were coupled to different fluorochromes, allowing the sorting of the two populations by FACS at a ratio of 9 immune cells to 1 tumoral cell. Cell suspensions were then loaded onto the 10X Genomics platform for single-cell capture. The raw data obtained were then processed using several bioinformatic analyses for genome alignment and quality control, and the results will be thoroughly discussed below.

Initial analysis of the cellular populations clustered in 11 groups shows the presence of all the expected immune cell populations infiltrating bladder cancer (**FIG. 9A**). Although some cell populations are not shown directly, they have been grouped as a broader category by the clustering algorithm (i.e., macrophages, monocytes, and neutrophils are not shown but are all categorized as the myeloid cluster). This is a limitation inherent to the high-dimensionality of the technique. scRNA-seq allows reading the top 20000 genes for expression for every cell, so it would be impossible to cluster cells in groups with biological meaning due to noise from non-informative or low-expressed genes. Feature selection allows us to reduce the number of these genes to only the ones that drive biological differences, and principal component analysis (PCA) identifies highly variable genes and reduces the gene set to a smaller set of principal components (PC), effectively reducing dimensionality. Single cells are then grouped together into clusters by algorithms that are based on the similarities between their respective PCs. Because this clustering process is essentially a mathematical approximation of biological complexity, and since the resolution of the clusters is arbitrary, it is entirely normal that some distinct

cell populations will separate well while others remain grouped. This is not a problem, since the initial clustering is primarily intended to confirm the presence of major cellular lineages and to assess possible broad transcriptomic shifts. When investigating changes in specific subpopulations, subsequent reclusterings are used. By isolating one or more specific clusters and repeating the feature selection and dimensionality reduction steps, a zoom-in of the populations of interest is obtained. Furthermore, although the samples were previously sorted for epithelial and immune lineages, as stated above, the emergence of a distinct fibroblast cluster (**FIG. 9A**), which belongs to the mesenchymal lineage, is still expected. In standard scRNA-seq analyses, clusters are ordered by size in decreasing order, so the fact that fibroblasts are the last cluster indicates they represent only a minute fraction of the total captured cells, and therefore they are likely a minor contamination from the cell sorting phase. By looking into the proportion of cells between NMIBC, MIBC, and papilloma per cluster (**FIG. 9C**), there is no major difference in the frequencies of the populations, apart from an increase in proliferating cells in NMIBC compared with MIBC. The only other notable difference is an increase in tumour cells in NMIBC compared with the other two groups (**FIG. 9C**). This does not reflect a true change in tumour-cell frequency; rather, it resulted from a manual error on our part, which led to some NMIBC samples containing more than the 10% tumour cells intended for analysis.

A

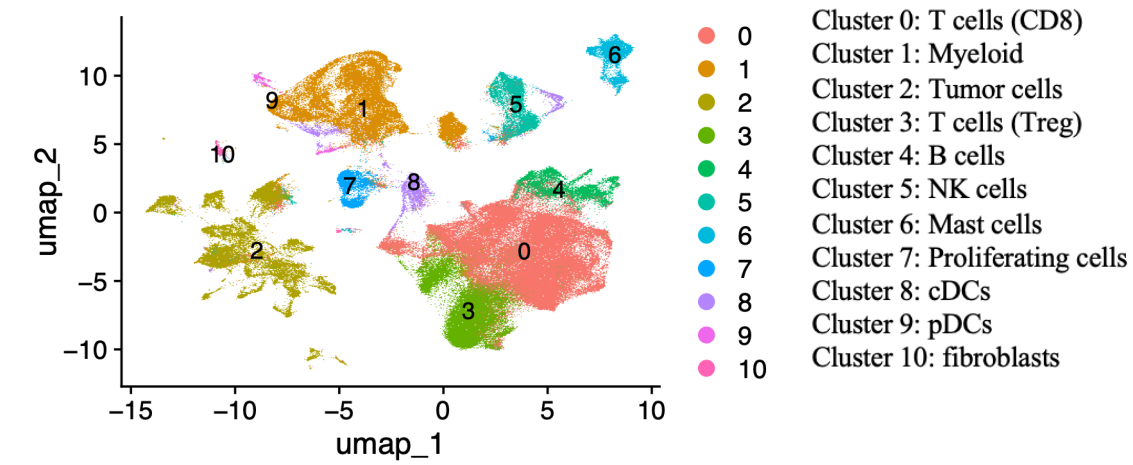
umap_2
umap_1
0
1
2
3
4
5
6
7
8
9
10
Cluster 0: T cells (CD8)
Cluster 1: Myeloid
Cluster 2: Tumor cells
Cluster 3: T cells (Treg)
Cluster 4: B cells
Cluster 5: NK cells
Cluster 6: Mast cells
Cluster 7: Proliferating cells
Cluster 8: cDCs
Cluster 9: pDCs
Cluster 10: fibroblasts

B

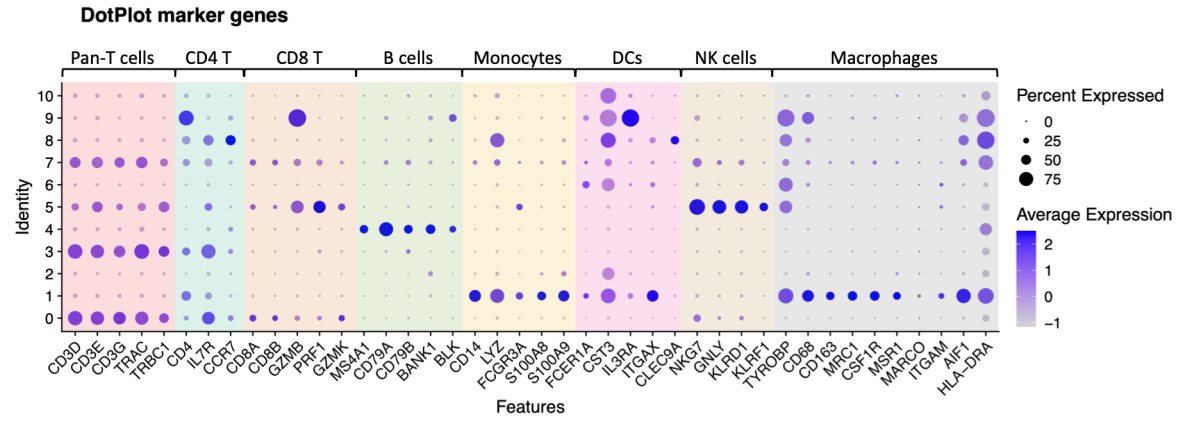
DotPlot marker genes
Pan-T cells
CD4 T
CD8 T
B cells
Monocytes
DCs
NK cells
Macrophages
Identity
Features
Percent Expressed
Average Expression
CD3D
CD3E
CD3G
TRAC
TRBC1
CD4
IL7R
CCR7
CD8A
CD8B
GZMB
PRF1
GZMK
MS4A1
CD79A
CD79B
BANK1
BLK
CD14
LYZ
FCGR3A
S100A8
S100A9
FCER1A
CST3
IL3RA
ITGAX
CLEC9A
NKG7
GNLY
KLRD1
KLRF1
TYROBP
CD68
CD163
MRC1
CSF1R
MSR1
MARCO
ITGAM
AIF1
HLA-DRA

C

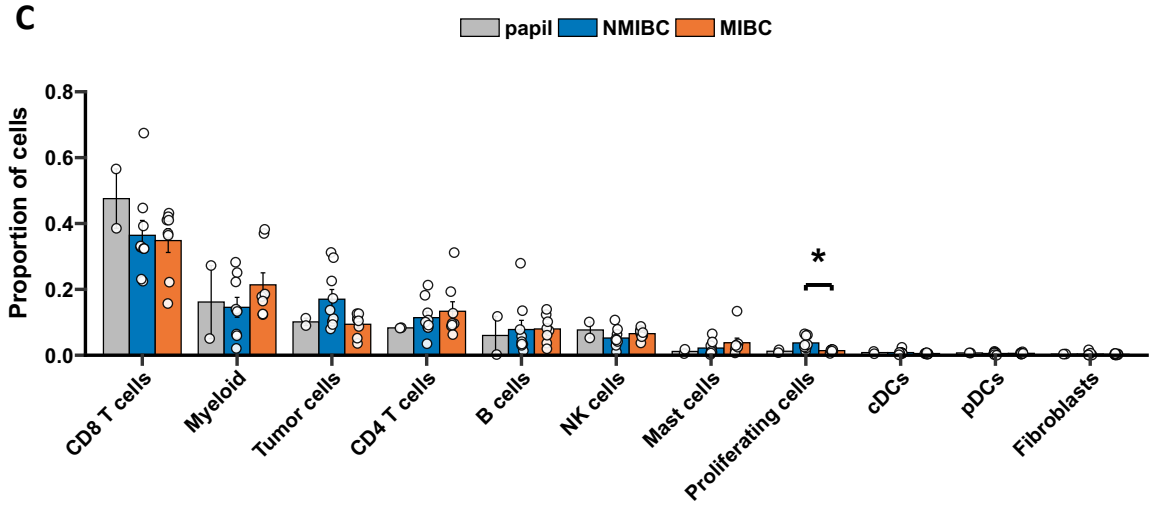
papil
NMIBC
MIBC
Proportion of cells
*
CD8 T cells
Myeloid
Tumor cells
CD4 T cells
B cells
NK cells
Mast cells
Proliferating cells
cDCs
pDCs
Fibroblasts

FIG. 9. **Single-cell RNA sequencing overview of the bladder tumor microenvironment.** (**A**) Uniform manifold approximation and projection (UMAP) of all cells in the scRNA-seq analysis. Single cells are visualized as dots, where the spatial proximity between dots represents their transcriptomic similarity. Closely grouped cells share highly similar gene expression profiles, while distinct lineages are separated by larger distances. The legend at the right shows all the clusters numbered from largest to smallest, with the colour code assigned in the UMAP and the name of the cellular population they represent. (**B**) Dotplot showing marker genes for the main immune lineages expected in the analysis. HLA-DRA, even if grouped with macrophage markers, is a marker for all professional antigen-presenting cells. (**C**) Bar plot showing the proportion of cells for each cluster in percentage (1.00=100%) with direct comparison of single clusters for NMIBC, MIBC, and papilloma. On top, the statistics for each comparison are shown, where * means that there is a statistical difference in frequency between the two tumours.

1.2 Immune populations reclusterings

Since this work is primarily concerned with the immune compartment, and given that the combined analysis did not reveal major differences between groups, we generated separate reclusterings for three major immune compartments: T+NK, myeloid, and B cells, to resolve their heterogeneity at higher resolution. Reclustering is a method in which selected clusters from the initial analysis are extracted, and the feature selection and PCA steps are then repeated using only these cells. Populations with similar transcriptional profiles are grouped together during the initial, coarse-grained analysis; isolating them removes the variance contributed by unrelated cell types, allowing the algorithm to resolve more subtle differences between sub-populations that are, in fact, transcriptionally distinct. First, the reclustering for the T+NK compartment (**FIG. 10A**). Within the CD4+ compartment we identified conventional CD4+ T cells, regulatory T cells, T follicular helper cells and Th17 cells; within the CD8+ compartment, effector CD8+ T cells, tissue-resident memory T cells and cytotoxic αβ/γδ T lymphocytes; and, among innate-like lymphocytes, NK cells and NK-like γδ T cells. A further cluster of cycling T cells could not be assigned to a single subset, since proliferating cells of different lineages converge on a shared transcriptional programme. Three additional clusters were not given a biological interpretation: a myeloid contamination that had been grouped with the lymphoid lineage at the resolution of the global clustering, a cluster defined by mitochondrial transcripts, and one defined by a stress-response signature, the latter belonging to the T lineage but characterized by a technical rather than a biological programme (**FIG. 10A**). Comparing the proportion of each subpopulation between the three groups (**FIG. 10B**), only two populations differ significantly between NMIBC and

MIBC: tissue-resident memory T cells, which contract in the muscle-invasive setting, and effector CD8+ T cells, which expand. All the remaining subpopulations are comparable between the two stages.

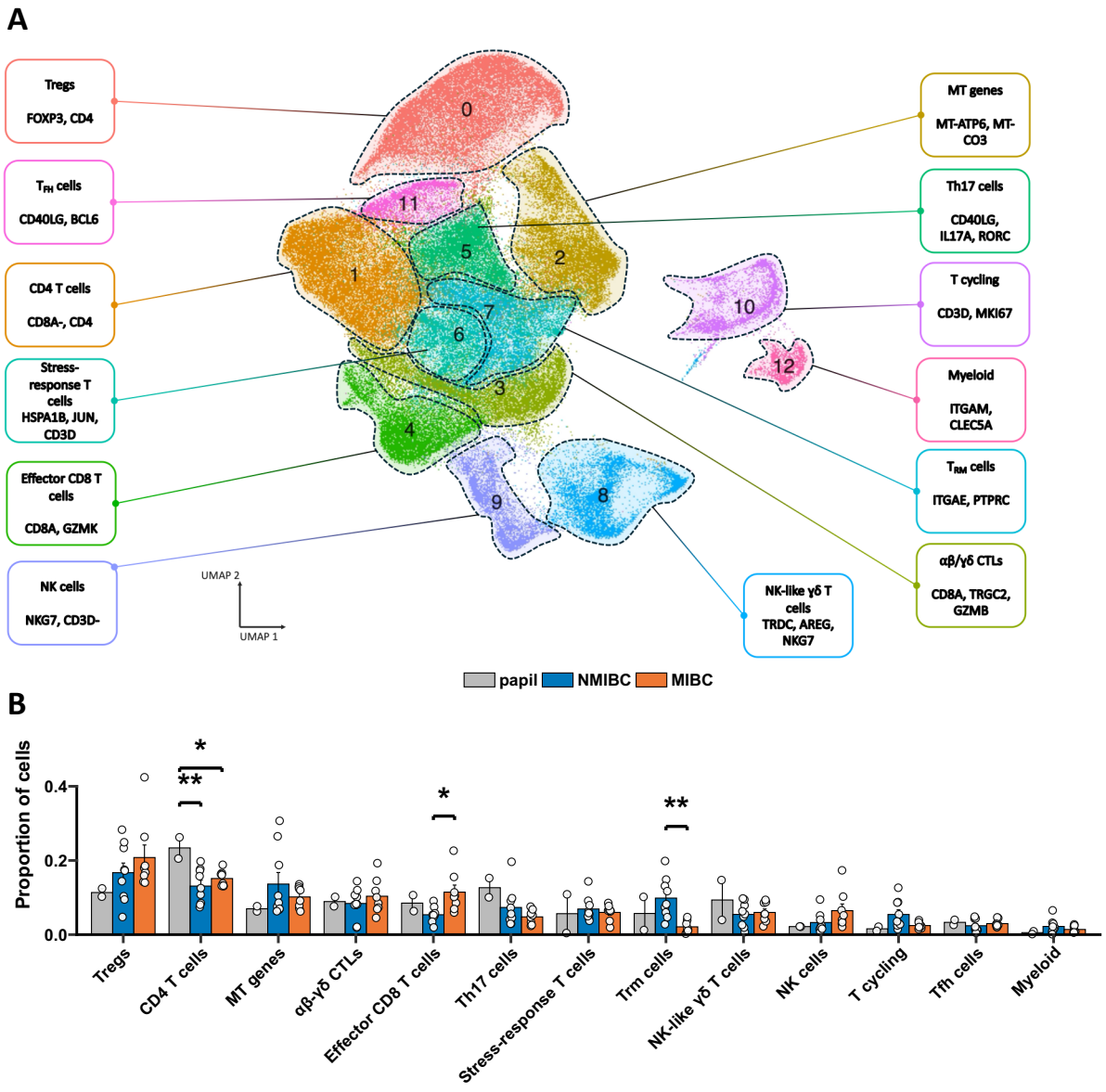

FIG. 10. **Reclustering of the T-NK compartment.** (**A**) UMAP of the T+NK reclustering. Clusters 0, 3, and 5 were extracted from the combined analysis, and the dimensionality reduction pipeline was run again with only them. (**B**) Bar plot showing the proportion of cells for each T/NK cluster in percentage (1.00=100%) with direct comparison of single clusters for NMIBC, MIBC, and papilloma.

Applying the same strategy used for the T + NK cell compartment, we reclustered the myeloid cells identified in the merged analysis (**FIG. 9A**) in order to resolve the subpopulations that remain indistinguishable at the resolution of the global clustering (**FIG. 11A**). This zoom-in separated the monocyte and macrophage compartment into CD14+ classical monocytes, CD16+ non-classical monocytes, M2-like macrophages and three transcriptionally defined tumour-associated macrophage (TAM) subsets, marked respectively by SPP1, TNFSF10 and FOLR2, alongside neutrophils and conventional dendritic cells (cDCs). As already seen in the T + NK cell reclustering, a few of the resulting clusters did not belong to the myeloid lineage, namely T cells and plasma cells, so these are reported for completeness but were not interpreted biologically (**FIG. 11A**). Direct comparison of the proportion of each subpopulation between the three groups (**FIG. 11B**) shows that the myeloid compartment of MIBC differs appreciably from that of NMIBC. CD14+ classical monocytes and neutrophils are significantly more represented in the muscle-invasive setting, with neutrophils displaying by far the largest shift, rising from a marginal fraction in NMIBC to approximately one-fifth of the whole myeloid compartment. This is mirrored by a significant contraction of M2-like macrophages and of cDCs. Notably, none of the three TAM subsets, nor CD16+ non-classical monocytes, differed significantly between NMIBC and MIBC, each of them accounting for less than 4% of the myeloid compartment in all three groups (**FIG. 11B**).

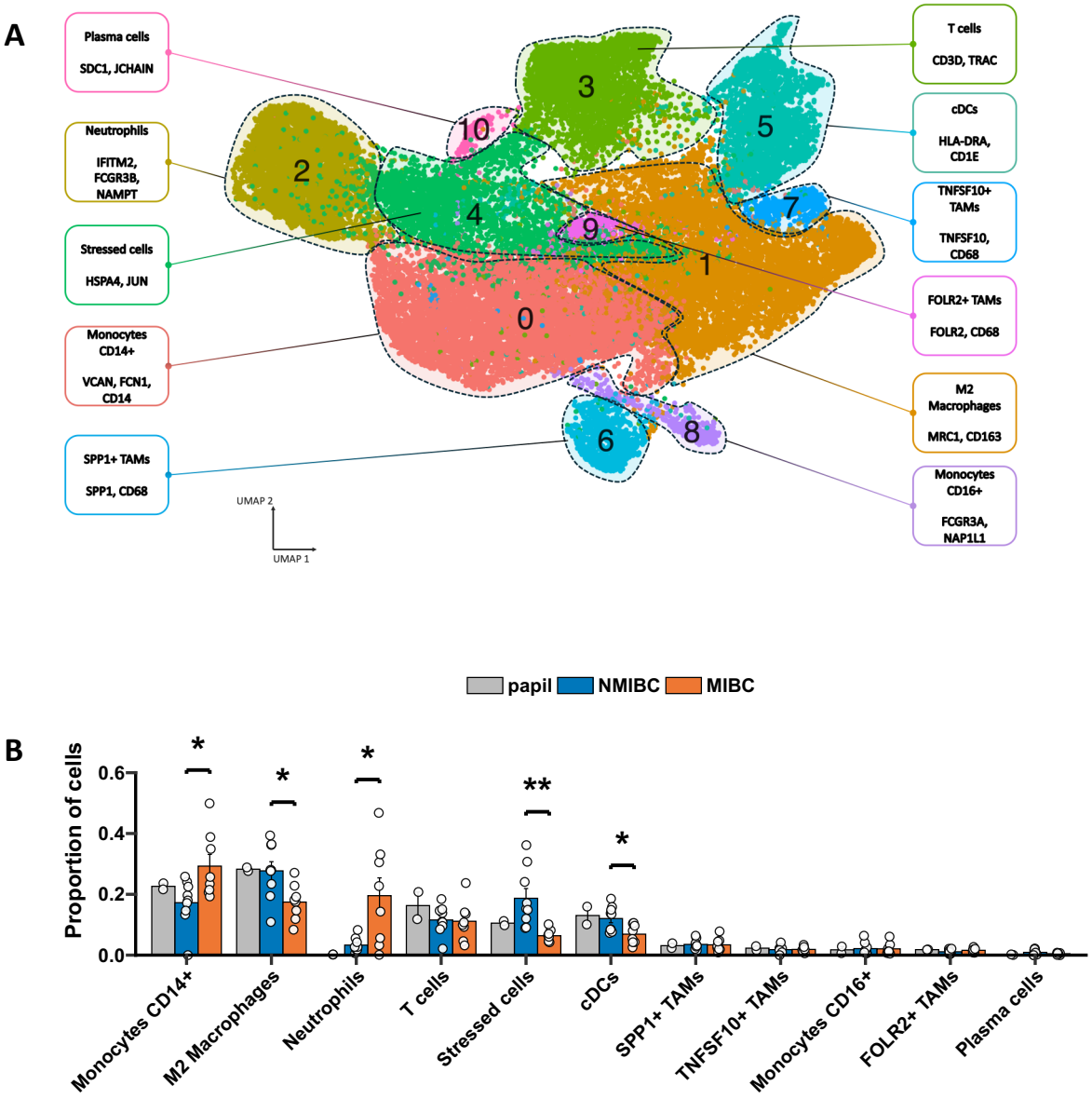

***FIG. 11*. Reclustering of the myeloid compartment.** (**A**) UMAP of the myeloid reclustering. Clusters 1, 6, 8, and 9 were extracted from the combined analysis, and the dimensionality reduction pipeline was run again with only them. (**B**) Bar plot showing the proportion of cells for each myeloid cluster in percentage (1.00=100%) with direct comparison of single clusters for NMIBC, MIBC, and papilloma.

We then turned to the B cell reclustering. This compartment was of particular interest: while higher B cell infiltration has been associated with a better prognosis in MIBC, the mechanisms underlying this association remain unclear, and the role of B cells in NMIBC is even less well characterized[110]. Within this compartment, activated B cells were higher in number in MIBC compared with NMIBC (**FIG. 12B**). Both activated and memory B cells were significantly reduced in the cancerous tissues compared with papilloma (**FIG.**

12B), although these comparisons should be interpreted with caution because of the limited number of papilloma samples (n=2). Moreover, this project's primary focus is the difference between invasive and non-invasive disease. Another shift became apparent when plasma cell clusters and non-plasma cell clusters were grouped together (**FIG. 12C**). Plasma cells were numerically increased in the cancerous tissues compared with papilloma, consistent with the expansion of the plasma cell compartment typically associated with malignancy. Within the two tumour groups, however, non-plasma B cells were numerically higher in MIBC than in NMIBC, and this difference was highlighted by the plasma/non-plasma ratio, which was correspondingly lower in MIBC (**FIG. 12C**). These data led us to suggest that B cells may show a defect in differentiation towards plasma cells specifically in the muscle-invasive carcinoma. It should be stressed, however, that everything described above rests exclusively on cell frequencies. Proportions derived from single-cell data are compositional in nature, so that the expansion of one population mechanically compresses all the others, and they are additionally sensitive to tissue dissociation, sample handling, and cell capture efficiency, which are not uniform across sample types. Frequency shifts of this kind are useful in indicating where to look, but on their own they do not establish that a population is functionally different between disease stages.

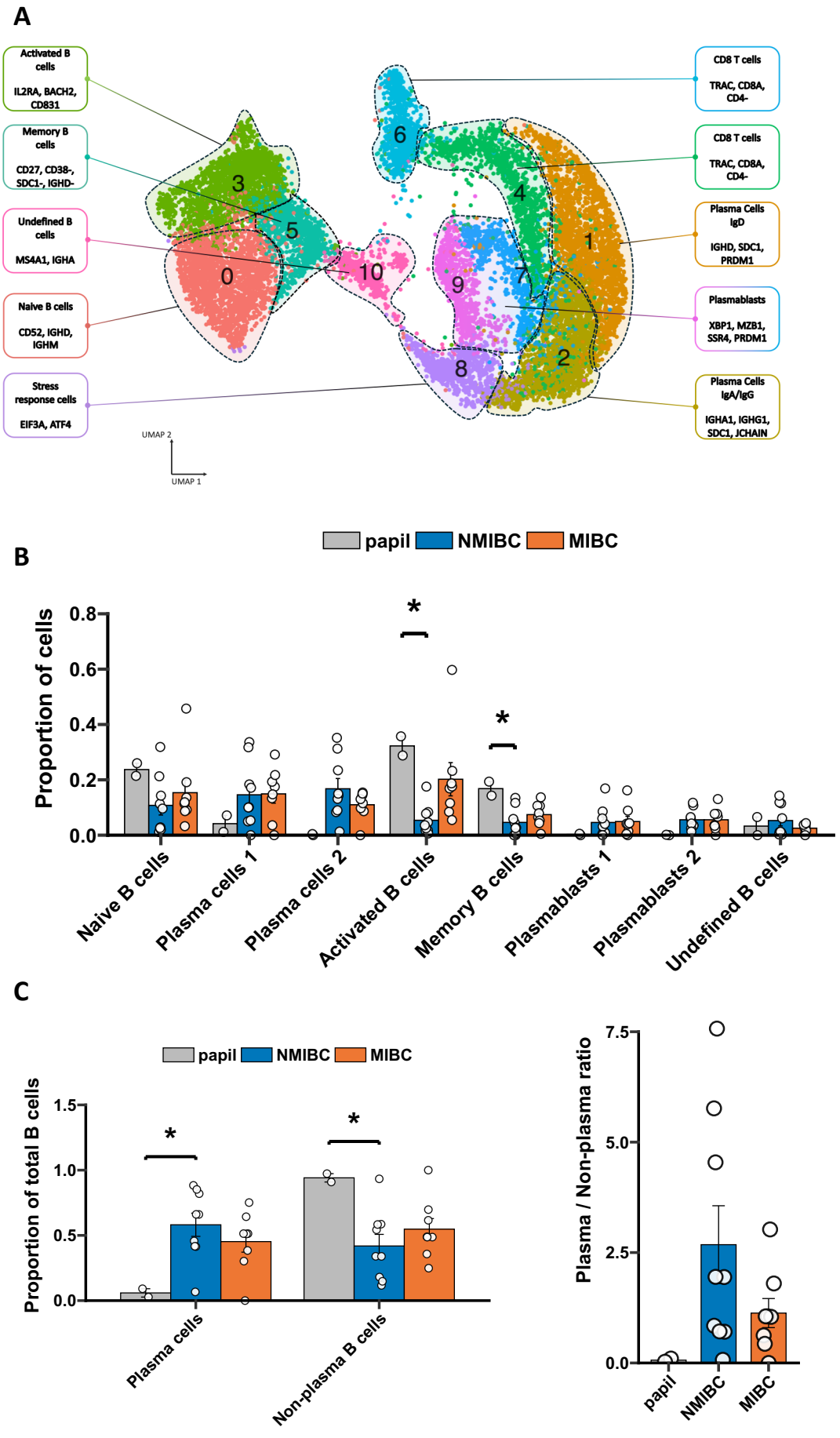
A
Activated B cells
IL2RA, BACH2, CD831
Memory B cells
CD27, CD38-, SDC1-, IGHD-
Undefined B cells
MS4A1, IGHA
Naive B cells
CD52, IGHD, IGHM
Stress response cells
EIF3A, ATF4
CD8 T cells
TRAC, CD8A, CD4-
CD8 T cells
TRAC, CD8A, CD4-
Plasma Cells IgD
IGHD, SDC1, PRDM1
Plasmablasts
XBP1, MZB1, SSR4, PRDM1
Plasma Cells IgA/IgG
IGHA1, IGHG1, SDC1, JCHAIN
0
1
2
3
4
5
6
7
8
9
10
UMAP 2
UMAP 1
B
papil
NMIBC
MIBC
Proportion of cells
0.0
0.2
0.4
0.6
0.8
*
*
Naive B cells
Plasma cells 1
Plasma cells 2
Activated B cells
Memory B cells
Plasmablasts 1
Plasmablasts 2
Undefined B cells
C
papil
NMIBC
MIBC
Proportion of total B cells
0.0
0.5
1.0
1.5
*
*
Plasma cells
Non-plasma B cells
Plasma / Non-plasma ratio
0.0
2.5
5.0
7.5
papil
NMIBC
MIBC

FIG. 12. **Reclustering of the B cell compartment.** (**A**) UMAP of the B cells reclustering. Cluster 4 was extracted from the combined analysis, and the dimensionality reduction pipeline was run again with only it. (**B**) Bar plot showing the proportion of cells for each B cluster in percentage (1.00=100%) with direct comparison of single clusters for NMIBC, MIBC, and papilloma. (**C**) Bar plots showing a comparison between papilloma, NMIBC, and MIBC for the sum of all non-plasma cells, comprising clusters 0, 3, 5, 10, and the same comparison for the sum of all plasma cells, comprising clusters 1, 2, 7, 9 (left); and showing a comparison between papilloma, NMIBC, and MIBC for the plasma cells/non-plasma cells ratio, calculated by dividing the sum of all plasma cell cluster frequencies by the sum of all non-plasma cell cluster frequencies (right).

1.3 B cells display a distinct transcriptional programme in muscle-invasive disease

To further investigate the functional shifts of B cells in MIBC compared with NMIBC, we performed differential gene expression (DEG) analysis, which identifies genes significantly up- or downregulated in the invasive carcinoma across all compartments. Among the genes upregulated in MIBC were CXCR4, a chemokine receptor guiding B cell positioning within lymphoid tissue, and CD83, a dendritic cell maturation marker that, within the B cell lineage, is expressed especially on activated B cells and on light-zone germinal centre B cells (**FIG. 13A**). Among the downregulated genes, the most statistically significant were JCHAIN, which encodes a small protein essential for the assembly of multimeric immunoglobulins, and GPR15, a chemoattractant receptor mediating lymphocyte homing to the large intestine and skin, expressed by effector and regulatory T cell subsets as well as by memory B cells and plasmablasts (**FIG. 13A**). We next performed pathway analysis, comparing our DEGs against publicly available databases of annotated pathways and their constituent genes, in order to infer which pathways are up- or downregulated in MIBC compared with NMIBC. The three most significantly enriched pathways among the upregulated genes all relate to the translational machinery (**FIG. 13B**); this result should be interpreted with caution, as ribosomal genes are a frequent confounder in this type of analysis. Ribosomal genes are numerous; they constitute a substantial fraction of the total transcriptome, and they are co-regulated as a block by common upstream regulators such as mTOR and MYC. As a consequence, even small shifts in translational activity move a large number of genes coordinately, which inflates both the enrichment score and the significance of the corresponding pathways. Other terms, such as interferon signalling and the CXCR4 pathway, are more modest in gene ratio and significance, but may be more informative regarding genuine functional

changes in B cells (**FIG. 13B**). Among the downregulated pathways, the top hit is asparagine N-linked glycosylation (**FIG. 13B**). This is of interest because N-linked glycosylation of immunoglobulins is required for their recognition by Fc receptors on other immune cells and for binding of the complement protein C1q[111]. A second pathway of interest is B cell receptor signalling, which is essential for B cell activation.

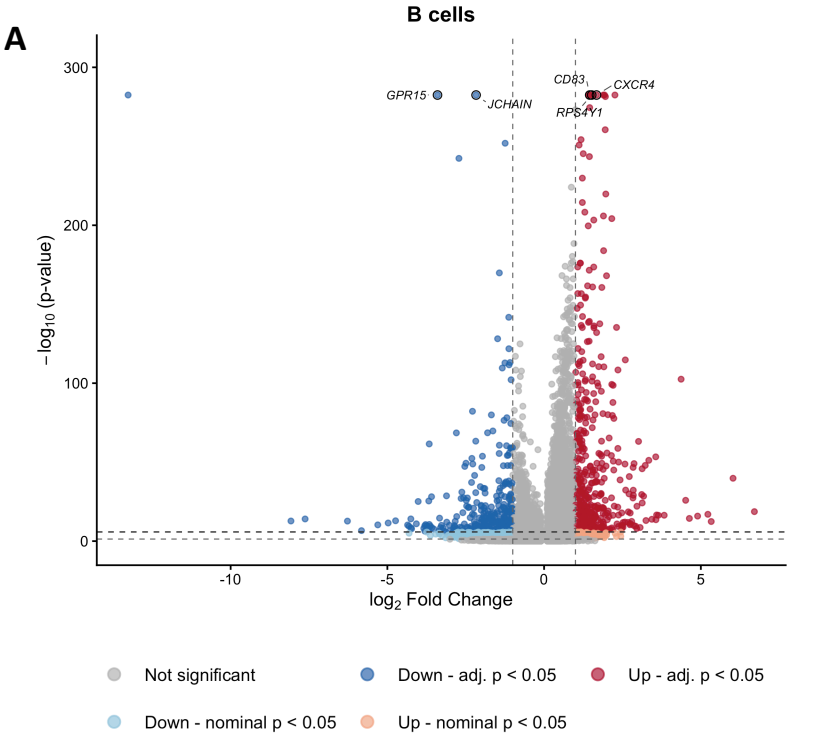
A
B cells
GPR15
JCHAIN
CD83
CXCR4
RPS4Y1
300
200
100
0
−log10 (p-value)
-10
-5
0
5
log2 Fold Change
Not significant
Down - adj. p < 0.05
Up - adj. p < 0.05
Down - nominal p < 0.05
Up - nominal p < 0.05

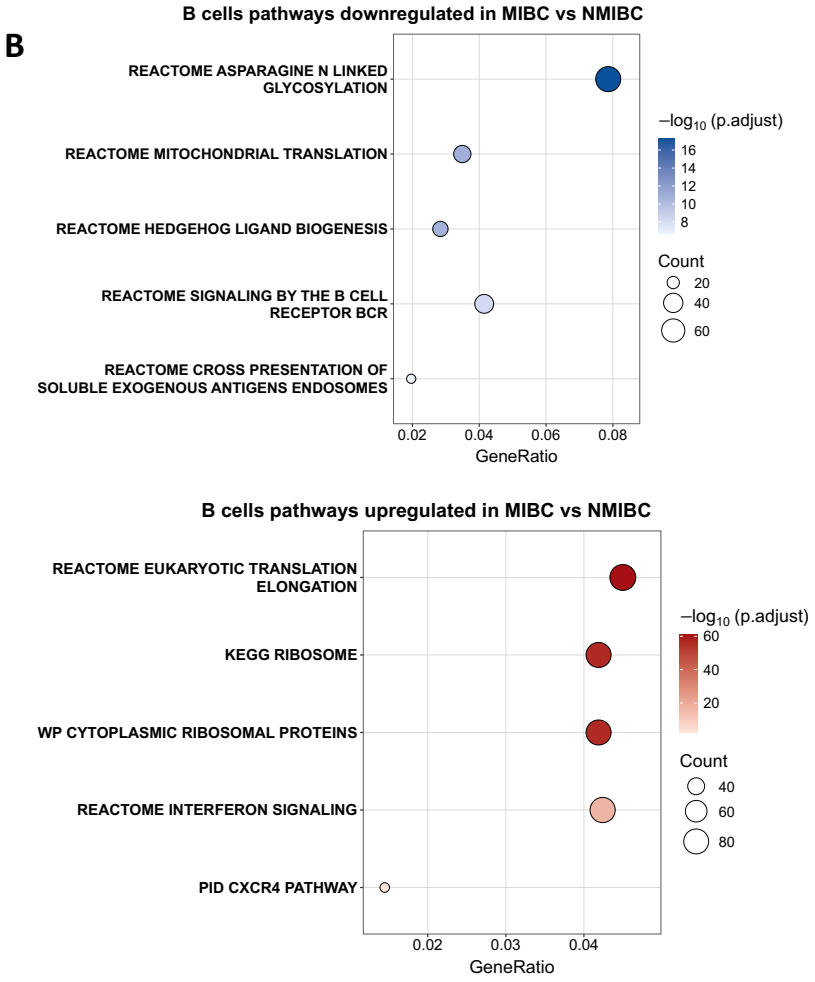
B
B cells pathways downregulated in MIBC vs NMIBC
REACTOME ASPARAGINE N LINKED GLYCOSYLATION
REACTOME MITOCHONDRIAL TRANSLATION
REACTOME HEDGEHOG LIGAND BIOGENESIS
REACTOME SIGNALING BY THE B CELL RECEPTOR BCR
REACTOME CROSS PRESENTATION OF SOLUBLE EXOGENOUS ANTIGENS ENDOSOMES
0.02
0.04
0.06
0.08
GeneRatio
−log10 (p.adjust)
16
14
12
10
8
Count
20
40
60
B cells pathways upregulated in MIBC vs NMIBC
REACTOME EUKARYOTIC TRANSLATION ELONGATION
KEGG RIBOSOME
WP CYTOPLASMIC RIBOSOMAL PROTEINS
REACTOME INTERFERON SIGNALING
PID CXCR4 PATHWAY
0.02
0.03
0.04
GeneRatio
−log10 (p.adjust)
60
40
20
Count
40
60
80

FIG. 13. **Differential gene expression and pathway enrichment in B cells, MIBC vs NMIBC.** (**A**) Volcano plot showing the top up- and downregulated genes in MIBC compared with NMIBC for p-value adjusted. Genes that don't change significantly are portrayed as grey dots, genes that change significantly for p-value, but not for p-value adjusted are shown in orange (upregulated) or light blue (downregulated), while genes that change significantly for p-value adjusted are shown in either red (upregulated) or blue (downregulated). There is also a threshold for showing only genes with a log2FC >1, meaning that their expression has to be at least double or half for them to appear. (**B**) Dot plots showing the top upregulated (left) and downregulated (right) pathways in MIBC compared with NMIBC. The greater the intensity of the colour, the lower is the p-value adjusted of the pathway, while the dots appear bigger based on the number of genes involved in the pathway and more at right based on GeneRatio (genes composing the pathway/total up/downregulated genes for that cell cluster).

1.4 Predicted ligand-receptor interactions across B cell subsets and tumour cells

Having characterised how the transcriptional programme of B cells differs between the two tumour groups, we next asked whether their interactions with the surrounding microenvironment, and with tumour cells in particular, were similarly altered. CellChat analysis was used to compare the number of inferred interactions across B cell clusters and between B clusters and the tumour in MIBC and NMIBC (**FIG. 14A**). CellChat infers intercellular communication from scRNA-seq data by quantifying the coordinated expression of ligand-receptor pairs, drawn from a curated interaction database, between each pair of clusters. Each cluster is thus considered both as a sender, expressing ligands, and as a receiver, expressing the corresponding receptors, yielding a predicted number of interactions for every sender-receiver combination. Most of the interactions increased in MIBC involved tumour cells and B cell clusters, in both directions. With tumour cells as senders, the main increases in MIBC were directed towards the plasma cell and plasmablast clusters, indicating that the tumour signals preferentially to the plasma cell compartment (**FIG. 14A**). With tumour cells as receivers, the populations showing the largest increases were undefined B cells, followed by activated B cells and plasmablasts (**FIG. 14A-B**) On the other hand, among the interactions increased in NMIBC, naive B cells were the main senders, showing more interactions with both tumour cells and all other B cell populations (**FIG. 14A**). As receivers, naive B cells also received more interactions in NMIBC from all B cell populations except undefined B cells, while interactions received from tumour cells were reduced. The strongest increase in NMIBC on the receiving side, however, was observed in undefined B cells, which received markedly more interactions from all other B cell clusters (**FIG. 14A**).

A

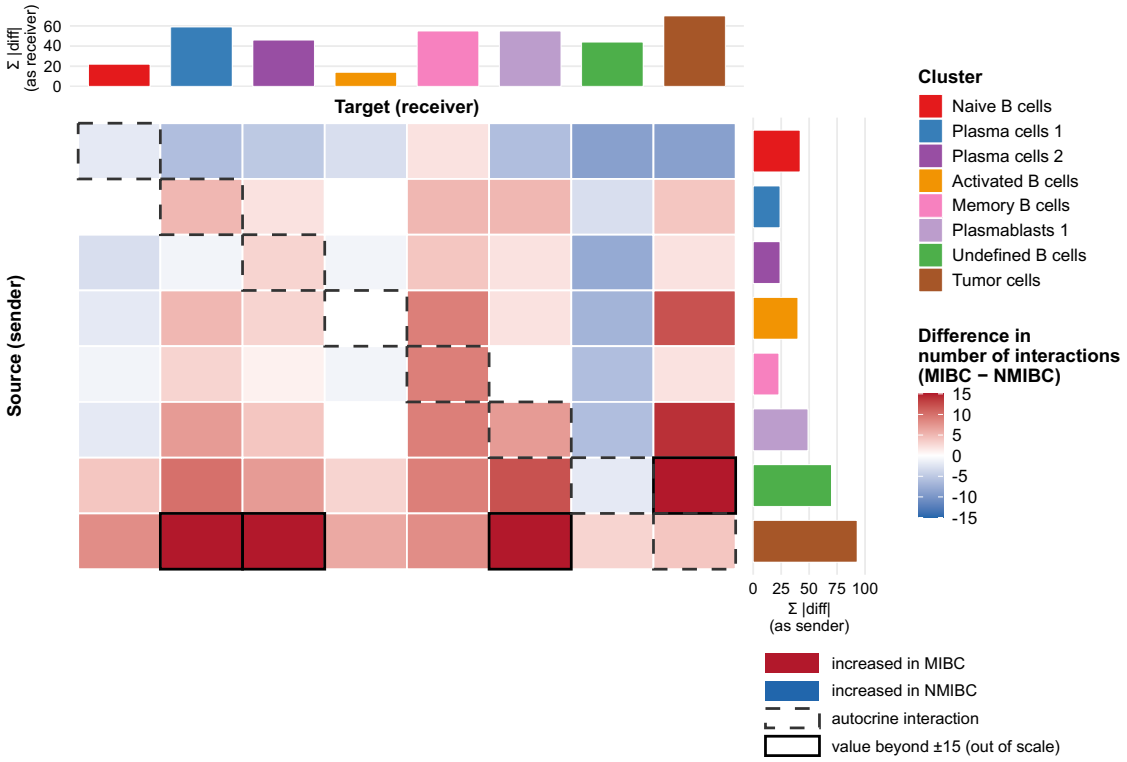
Difference in the number of interactions: MIBC vs NMIBC
Σ |diff| (as receiver)
60
40
20
0
Target (receiver)
Source (sender)
0 25 50 75 100
Σ |diff| (as sender)
Cluster
Naive B cells
Plasma cells 1
Plasma cells 2
Activated B cells
Memory B cells
Plasmablasts 1
Undefined B cells
Tumor cells
Difference in number of interactions (MIBC − NMIBC)
15
10
5
0
-5
-10
-15
increased in MIBC
increased in NMIBC
autocrine interaction
value beyond ±15 (out of scale)

B

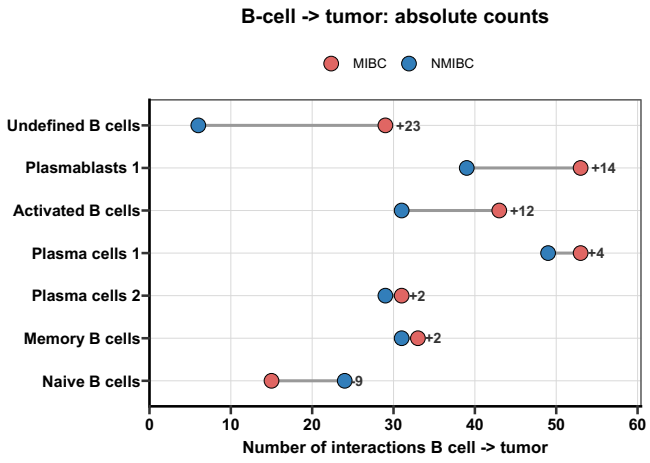
B-cell -> tumor: absolute counts
MIBC
NMIBC
Undefined B cells
Plasmablasts 1
Activated B cells
Plasma cells 1
Plasma cells 2
Memory B cells
Naive B cells
+23
+14
+12
+4
+2
+2
-9
0
10
20
30
40
50
60
Number of interactions B cell -> tumor

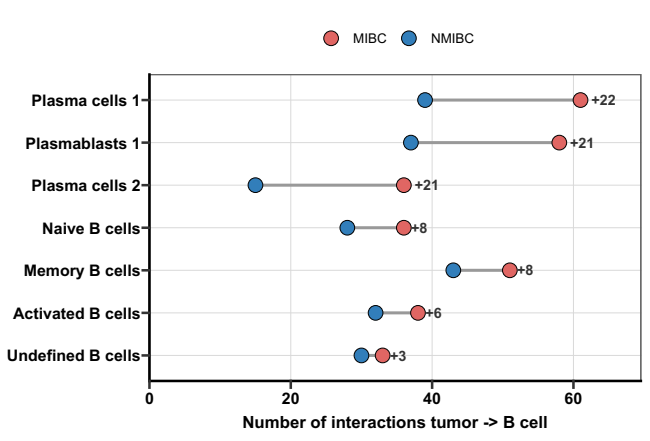
Tumor -> B-cell: absolute counts
MIBC
NMIBC
Plasma cells 1
Plasmablasts 1
Plasma cells 2
Naive B cells
Memory B cells
Activated B cells
Undefined B cells
+22
+21
+21
+8
+8
+6
+3
0
20
40
60
Number of interactions tumor -> B cell

FIG. 14. **Predicted cell–cell communication between B cell subsets and tumour cells in MIBC and NMIBC.** (**A**) Heatmap showing the difference in the number of inferred interactions between MIBC and NMIBC (MIBC - NMIBC) for each sender-receiver pair; rows represent the signal-sending cluster and columns the signal-receiving cluster. Red indicates interactions increased in MIBC, blue interactions increased in NMIBC. Dashed outlines mark autocrine interactions, solid outlines mark values exceeding the +-15 colour scale. The bar plots on the top and right summarise the total absolute difference in interactions for each cluster as receiver and as sender, respectively. **(B)** Number of inferred interactions between each B cell subset and tumour cells (high) and between tumour cells and each B cell subset (low); numbers indicate the difference in the inferred interactions between MIBC and NMIBC.

2. Impact of the bladder cancer secretome on B cell maturation and differentiation

2.1 Conditioning of B cells with bladder tumour secretoma

The increase in predicted tumour-to-B cell signalling in MIBC raised the question of what effect tumour-derived signals actually exert on B cells. This question was made all the more relevant by the impairment of plasma cell differentiation suggested by both the shift in plasma/non-plasma composition and the downregulation of BCR signalling and of the secretory machinery. Since our primary interest lies in how the tumour microenvironment as a whole shapes infiltrating immune cells, rather than in direct cell-to-cell contact, we chose to address this experimentally by isolating the soluble component of tumour signalling, using conditioned medium from a bladder cancer cell line, which captures the secreted fraction of the interactions inferred above. Therefore, splenic B cells isolated from C57BL/6 mice were cultured for 24 hours with conditioned medium (CM) collected from the MB49 murine bladder cancer cell line, or with control medium (**FIG. 15A**). B cells were then stained with a panel of fluorochrome-conjugated antibodies directed against lineage and functional markers, and analysed by flow cytometry. The gating strategy used for all flow cytometry analyses in this and the following experiments is shown in FIG. 15B. Compared with control, CM reduced B cell viability, although both conditions retained well over 50% live cells (**FIG. 15C**). CM also modestly reduced the

percentage of transitional B cells, while the mature compartment remained unchanged (**FIG. 15C**). Within the transitional compartment (comprising T1 and T2, which represent sequential maturation stages, and T3, which is largely composed of anergic cells that fail to reach the mature state) CM reduced both the T2 and the T3 fractions, but this decrease was not accompanied by an increase in T1 transitional B cells (**FIG. 15D**). The population that was actually increasing was the IgM- CD23- double negative transitional B cells, which have not been reported in literature (**FIG. 15D**). The percentage of plasma cells among B cells was also reduced by CM, although plasma cells represented only a minute fraction of total B cells in both conditions, as they require specific stimulation to differentiate consistently (**FIG. 15C**). The percentage of Bregs (TGF-β+ PD-L1+ cells among CD5+ B cells) did not differ between conditions (**FIG. 15C**). Functional markers were assessed as mean fluorescence intensity (MFI) on total B cells. PD-L1, a marker of immunosuppressive phenotype, showed no difference between conditions, whereas MHC-II, a marker of antigen presentation, was increased in the CM condition (**FIG. 15E**). Strikingly, and in line with the transcriptomic data described above, CXCR4 MFI was markedly increased by CM exposure, the most pronounced change observed in this experiment (**FIG. 15E**).

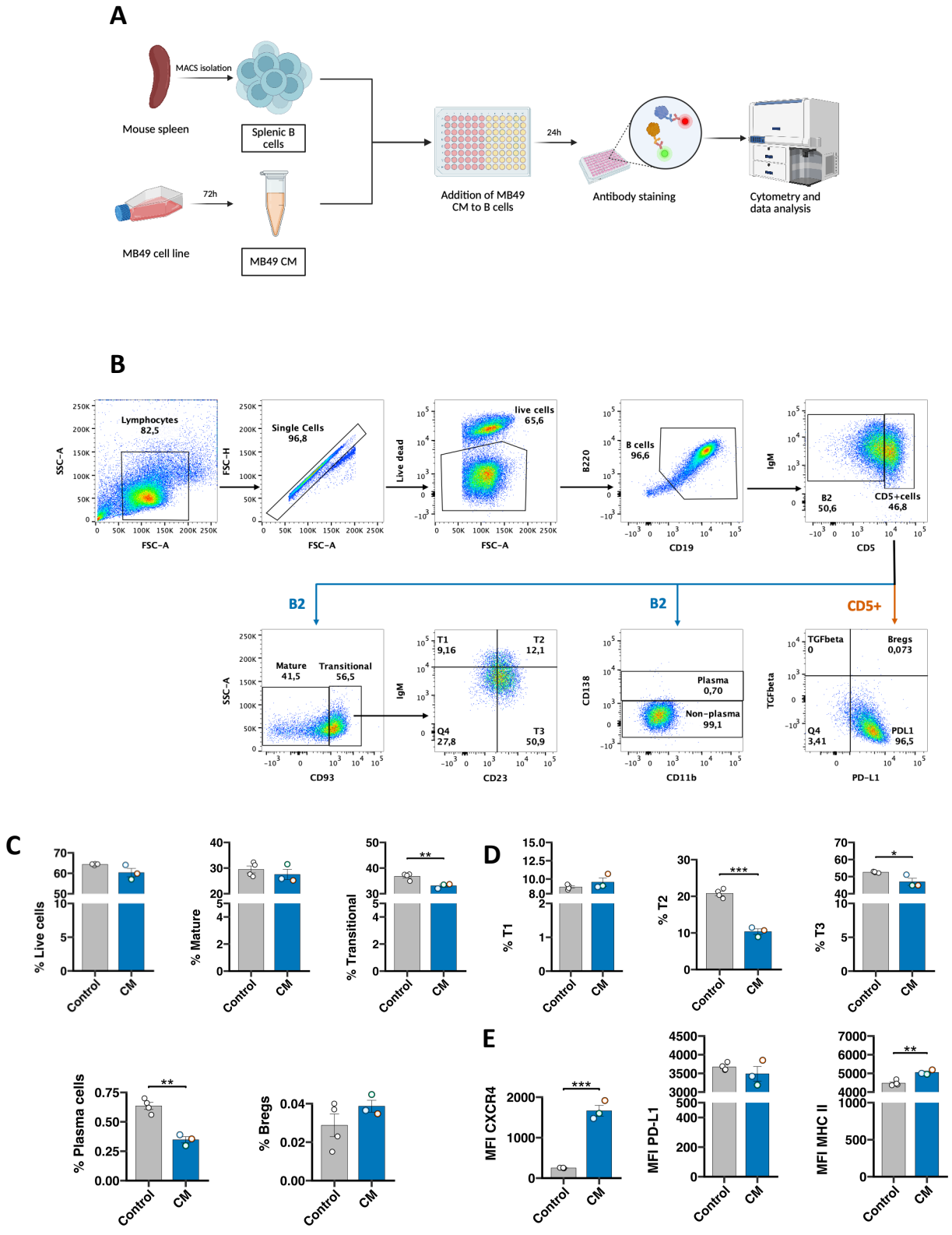

FIG. 15. **Effect of MB49 conditioned medium on splenic B cells *in vitro*.** (**A**) Experimental plan of *in vitro* conditioning of mouse B cells. (**B**) Gating strategy applied to the data obtained through FACS. (**C**) Bar plots showing the shifts in B cell vitality, and frequencies of all the populations gated in B cells between culture medium and control. (**D**) Bar plots showing transitional B cells subpopulations. (**E**) Bar plots showing functional markers in B cells.

2.2 Conditioning of induced plasma cells with bladder tumour secretoma

To obtain a complete overview of how MB49 CM shapes B cell behaviour, we designed a second *in vitro* experiment in which splenic B cells were stimulated to differentiate into plasma cells, allowing us to assess how CM influences this process. As a stimulation source, we adopted a dual approach, stimulating B cells with either lipopolysaccharide (LPS) or CD40 ligand (CD40L) (**FIG. 16A**). LPS was used to recapitulate the T-independent differentiation pathway, as it is recognised by TLR4 and elicits a strong cascade leading to B cell activation and plasma cell differentiation. CD40L, by contrast, was used to recapitulate the T-dependent pathway, in which T follicular helper cells provide co-stimulation. B cells were harvested from mouse spleens and cultured with LPS or CD40L, in the presence or absence of CM, for 72 hours (**FIG. 16A**). Samples were then stained with an antibody panel and analysed by flow cytometry (**FIG. 16A**). LPS induced a strong wave of plasma cell differentiation, and the addition of MB49 CM significantly hindered this process (**FIG. 16C**). CD40L, by contrast, did not increase the proportion of plasma cells compared with control; nonetheless, the inhibitory effect of the conditioned medium was still apparent, with CD40L+CM showing a reduction relative to both the control and the CD40L alone group (**FIG. 16C**). Examining the plasma cell compartment in more detail, antibody-secreting cells (ASC), defined as $CD38^{+}CD27^{-}$ plasma cells, were markedly reduced by LPS stimulation, with CM minimally restoring this loss; in the CD40L arm the reduction was far more modest, and the addition of CM decreased the ASC fraction further (**FIG. 16D**). Antibody-forming cells (AFC), defined as $CD27^{+}CD38^{-}$ plasma cells, represented only a minor fraction across all conditions and showed divergent responses in the two arms: LPS strongly increased AFC, an effect that was reduced by the addition of CM, whereas CD40L alone produced no increase and the combination of CD40L and CM raised the AFC fraction, opposite to what was observed in the LPS arm (**FIG. 16D**). It should be noted, however, that when dealing with such small populations, statistically significant shifts may correspond to differences of limited biological relevance. Finally, plasmablasts (PB), defined as $CD38^{+}CD27^{+}$ plasma cells, were reduced by LPS stimulation relative to control, whereas CD40L increased this population; in the CD40L arm, the addition of CM reduced PB back towards control levels (**FIG. 16D**). Overall, MB49 CM hinders B

cell differentiation into plasma cells, as the stimulated groups cultured with CM show plasma cell frequencies similar to, or lower than, those of the unstimulated control. Within the plasma cell compartment, however, the effect of CM is stimulus-dependent: in the LPS arm the CM-treated groups tend to revert towards an unstimulated-like phenotype, whereas in the CD40L arm CM shifts the compartment along a distinct trajectory, most notably by further increasing the AFC fraction.

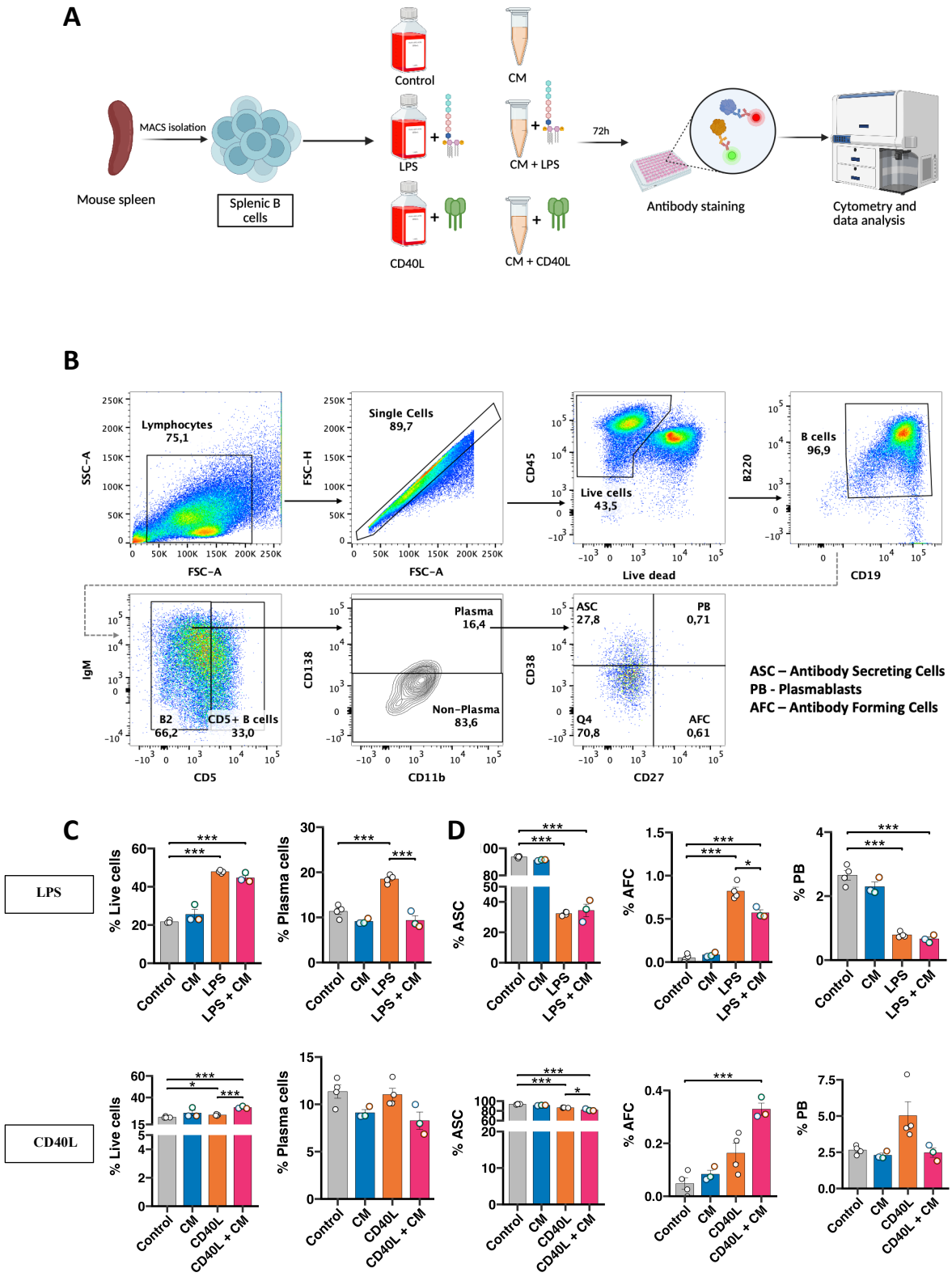

FIG. 16. **Effect of CM on LPS- and CD40L-driven B cell differentiation in plasma cells.** (**A**) Experimental plan of *in vitro* plasma cell derivation from mouse B cells and conditioning. (**B**) Gating strategy applied to the data obtained through cytometry. (**C**) Bar plots showing B cells vitality and the shifts in plasma cell frequencies. (**D**) Bar plots showing plasma cell subpopulations frequencies.

3. CXCR4 upregulation is also observed in the patient scRNA-seq dataset

Given the marked and consistent upregulation of CXCR4 observed both in the transcriptomic comparison of MIBC and NMIBC B cells and following CM exposure in vitro, CXCR4 expression was re-examined across the original patient scRNA-seq dataset, in a population- and subset-resolved manner, to determine whether this shift is specific to the B cell compartment or shared across the tumour microenvironment, and which B cell subsets drive it (**FIG. 17A**). Across the full cluster set, CXCR4 was upregulated in MIBC relative to NMIBC in most populations, but the most pronounced change was observed in B cells (**FIG. 17A**). CXCR4 was therefore not only among the top upregulated genes and pathways within the B cell compartment (**FIG. 13A-B)**, but B cells were also the population showing the strongest upregulation of this receptor in MIBC relative to NMIBC. Within B cell subsets, CXCR4 upregulation in MIBC was most pronounced in plasma cells 1, followed by naive and memory B cells, whereas undefined B cells showed the opposite direction, with higher expression in NMIBC (**FIG. 17B**). Interestingly, the other plasma cell cluster did not show any difference in CXCR4 expression between NMIBC and MIBC.

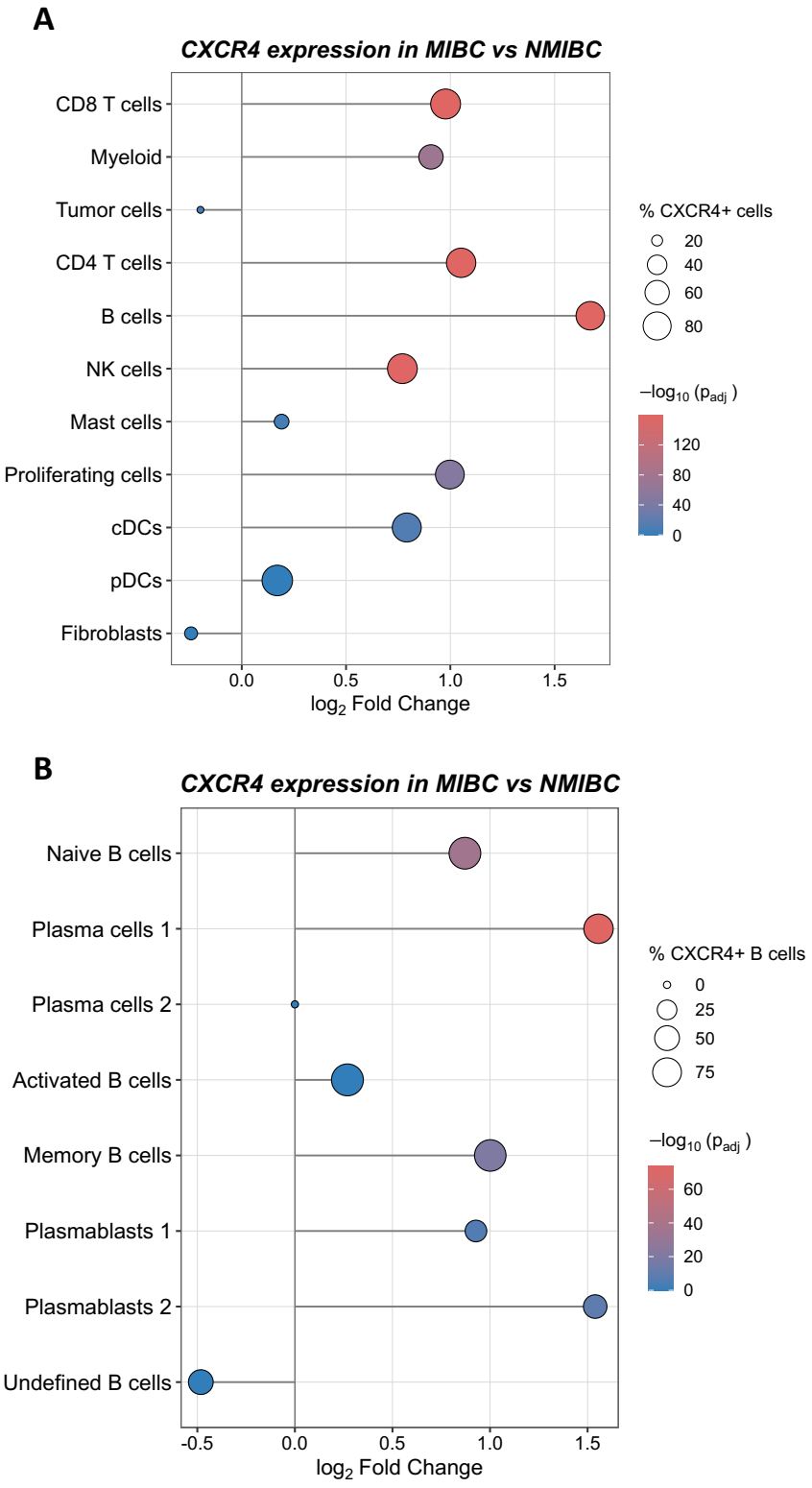
A
CXCR4 expression in MIBC vs NMIBC
CD8 T cells
Myeloid
Tumor cells
CD4 T cells
B cells
NK cells
Mast cells
Proliferating cells
cDCs
pDCs
Fibroblasts
0.0
0.5
1.0
1.5
log2 Fold Change
% CXCR4+ cells
20
40
60
80
–log10 (padj)
120
80
40
0
B
CXCR4 expression in MIBC vs NMIBC
Naive B cells
Plasma cells 1
Plasma cells 2
Activated B cells
Memory B cells
Plasmablasts 1
Plasmablasts 2
Undefined B cells
-0.5
0.0
0.5
1.0
1.5
log2 Fold Change
% CXCR4+ B cells
0
25
50
75
–log10 (padj)
60
40
20
0

FIG. 17. **CXCR4 expression in MIBC compared with NMIBC across immune populations and B cell subsets.** (**A**) Log2 fold change of CXCR4 expression in MIBC relative to NMIBC, shown for all clusters of the combined analysis and (**B**) for the B cell subsets identified in the B cell reclustering. Positive values indicate higher expression in MIBC. Dot size represents the percentage of CXCR4-expressing cells within each population, and dot colour the -log10 of the adjusted p-value.

4. In vivo validation in the BBN carcinogen-induced model of bladder cancer

As a final step, and to determine whether the phenotypes described above could also be captured in a whole-organism setting, the BBN carcinogen-induced mouse model of bladder cancer was employed. Male C57BL/6 mice were treated with the carcinogen N-butyl-N-(4-hydroxybutyl)nitrosamine (BBN) in drinking water for 12 weeks, a model previously shown to recapitulate the histological and molecular features of bladder cancer. BBN-treated mice and water-only controls, each comprising two independent cohorts, were sacrificed at an early (week 16) or late (week 24) time point, corresponding to the NMIBC-like and MIBC-like stages of tumour progression, respectively. Bladder tissue was then analysed by flow cytometry (**FIG. 18A**). The percentage of live cells and of B cells among $CD45^+$ cells did not differ significantly between control and treated groups, although B cell infiltration was generally higher at the late time point in both (**FIG. 18B**). Within the B cell compartment, the percentage of mature B cells was reduced in BBN-late compared with control-late mice, differently from the *in vitro* CM exposure (**FIG. 18B**). The reduction in mature B cells at a late timepoint is consistent with an impairment of B cell differentiation affecting multiple stages, rather than the plasma cell transition alone. The percentage of transitional B cells was likewise reduced, although in this case the difference was restricted to the early time point, with no difference between BBN-late and control-late mice (**FIG. 18B**). Within the transitional compartment, the T1 fraction was higher and the T2 fraction correspondingly lower at both late time points compared with both early time points, but no difference was found between control and treated animals; this redistribution therefore tracked with time point rather than with BBN treatment, and does not reproduce the CM-driven shift towards T1 observed in vitro. The T3 fraction remained negligible throughout (**FIG. 18B**). The percentage of plasma cells

among B cells was reduced in BBN-late compared with control-late mice, in line with the reduction in plasma cells observed both under CM exposure alone and upon stimulation with LPS or CD40L in the presence of CM (**FIG. 18B**). The percentage of Bregs did not differ significantly between groups, as was also the case *in vitro* (**FIG. 18B**). Among the functional markers, the percentage of MHC II-high B cells was reduced in BBN-late compared with control-late mice, in contrast with the increase in MHC II observed in B cells exposed to CM in vitro (**FIG. 18B**). The percentage of CXCR4-high B cells was reduced in BBN-early compared with control-early mice; this finding diverges from the marked induction of CXCR4 by CM in vitro and from its upregulation in MIBC relative to NMIBC in the patient dataset (**FIG. 18B**). Finally, the percentage of PD-L1-high B cells was increased in BBN-late compared with control-late mice, a difference that was not apparent in the in vitro system, where PD-L1 was unchanged by CM exposure (**FIG. 18B**).

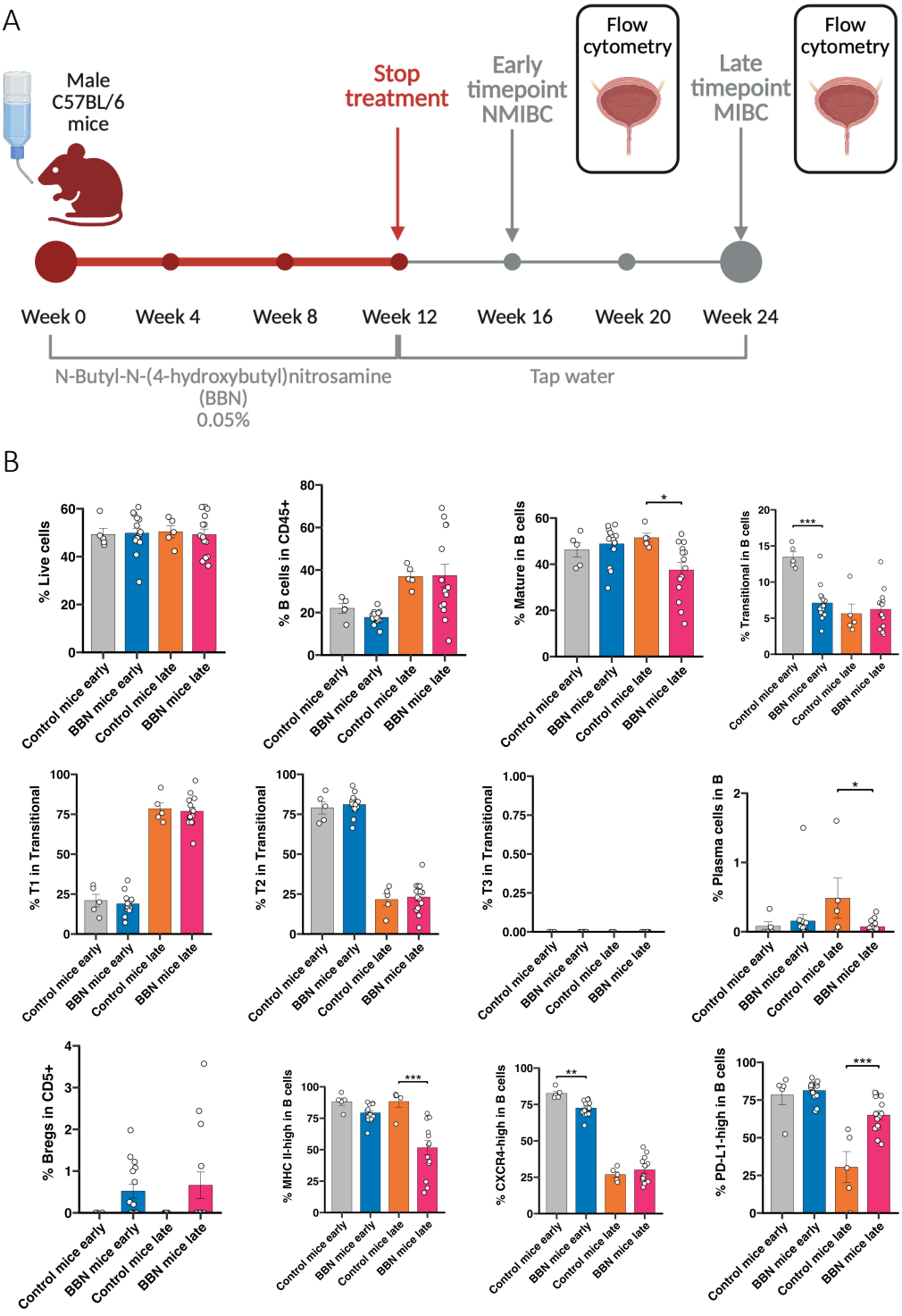

FIG. 18. **In vivo characterization of bladder B cells in the BBN model.** (**A**) BBN treatment schedule and tissue collection timepoints. (**B**) Frequencies of the indicated B-cell subsets and marker-high fractions in control and BBN-treated mice at early (week 16) and late (week 24) timepoints.

DISCUSSION

The transition from non-muscle-invasive to muscle-invasive bladder cancer marks a decisive change in clinical trajectory, yet the immunological events that accompany, and possibly enable, this transition remain only partially defined. The bladder tumour microenvironment as a whole has been described as understudied, with research effort historically concentrated on genetic and epigenetic alterations within the urothelial compartment rather than on the surrounding stroma and immune infiltrate[39]. Within the immune compartment, this imbalance is even more pronounced for B cells: while the T cell landscape of bladder tumours is now well characterised, the contribution of B cells to anticancer immunosurveillance remains less explored[112]. While the prognostic value of infiltrating B cells in MIBC is beginning to emerge, their role in NMIBC remains mostly to be defined, and the mechanisms governing B cell interactions with the tumour at all stages are still poorly understood[112]. In this work, we combined single-cell RNA sequencing of patient tumours with *in vitro* and *in vivo* experimental models to characterise the immune microenvironment across the non-invasive-to-invasive spectrum of bladder cancer. Although the overall composition of the immune infiltrate was largely comparable between groups, higher resolution analysis of the B cell compartment revealed a consistent set of alterations: a shift in the balance between plasma and non-plasma B cells, accompanied by transcriptional downregulation of programmes required for antibody production and secretion, and by a strong upregulation of CXCR4. These observations were reproduced experimentally, since exposure of murine splenic B cells to bladder tumour conditioned medium impaired plasma cell differentiation, while strongly inducing CXCR4, and were partially recapitulated in a carcinogen-induced *in vivo* model. The B cell compartment was not, however, the only one in which reclustering revealed differences between the two tumour groups, and the decision to focus on it therefore requires some justification. Sub-clustering of the T/NK compartment revealed changes that are of interest in themselves. Tissue-resident memory (Trm) T cells were reduced in MIBC relative to NMIBC, a shift consistent with the existing literature: a positive correlation between Trm infiltration and lower tumour stage has been reported in urinary bladder cancer[113]. Our observation is therefore in line with expectation and further supports previous findings. Effector CD8 T cells were instead increased in MIBC.

A direct comparison of effector CD8 frequencies between NMIBC and MIBC does not appear to have been reported in the literature, but the direction we observe is compatible with what is known about the mutational landscape of invasive and non-invasive bladder cancer and with the reported behaviour of CD8 T cells in that context. Mutational burden is higher in MIBC than in NMIBC[114], and within MIBC, subtypes with high mutational and neoantigen burden show greater infiltration by effector rather than exhausted CD8 T cells[115]. We therefore present this finding as consistent with the existing literature, although direct confirmation would require a dedicated comparison between the two groups. The same reclustering strategy applied to the myeloid compartment returned a coherent picture of the muscle-invasive transition: a significant expansion of classical CD14+ monocytes and, above all, of neutrophils in MIBC, mirrored by a relative loss of M2-like macrophages and conventional dendritic cells. Read together, these shifts depict a myeloid infiltrate that moves away from differentiated, antigen-presenting and tissue-associated populations and towards recently recruited, immature effectors, a picture that would fit well with the immune-excluded and immune-desert phenotypes frequently described in bladder cancer. The direction of most of these changes, and particularly the enrichment in tumour-associated neutrophils, is already documented for the transition to muscle-invasive disease [116], so that the added value of a purely compositional description would have been limited. Second, the subsets for which a functional characterization would have been most informative, namely the SPP1+, TNFSF10+ and FOLR2+ TAMs, each account for less than 4% of the myeloid compartment, a range in which compositional analyses are known to be severely underpowered with the number of biological samples available here[117]. Despite these observations, the B cell compartment was selected for in-depth investigation for two reasons. The first is that cell population proportions derived from scRNA-seq data are intrinsically noisy, and tests applied to such proportions are prone to detecting differences of limited biological meaning[118]. As performing a reclustering increases the number of populations tested, the probability of encountering isolated significant differences increases accordingly. Frequency shifts alone are therefore weak evidence and become informative mainly when supported by other layers of data. The second reason follows the same line of thought. Within the B cell compartment, the frequency shift was accompanied by a coherent transcriptional signature and by an altered pattern of predicted interactions with tumour cells. No

comparable convergence was available for the T/NK or myeloid findings, which remain a parallel line of investigation that we did not pursue further here. Several independent observations point towards a compromised transition of B cells into antibody-secreting cells in muscle-invasive disease. First, the data across the three groups in the scRNA-seq analysis described two distinct events, which should be read separately. Relative to papilloma, the plasma cell compartment was expanded in both malignant groups: this is the expected consequence of immune recognition of a malignant lesion, and its presence supports the biological coherence of the dataset[119]. The finding of interest lies within the malignant groups, where the plasma/non-plasma ratio was highest in NMIBC and lower in MIBC. The impairment we describe is therefore defined relative to non-muscle-invasive disease rather than relative to non-tumoural tissue. Second, the transcriptional profile of MIBC B cells showed downregulation of JCHAIN, which encodes the joining chain required for the assembly of multimeric immunoglobulins, coupled with downregulation of asparagine N-linked glycosylation. Variable domains of antibodies may acquire N-linked glycans during somatic hypermutation, and it was previously demonstrated by van de Bovenkamp et al.[120] how variable domains possessing this type of modification may be positively selected during affinity maturation and that they are associated with greater antigen binding capacity. Both of these findings lead towards an impaired functionality of B cells, especially more mature and differentiated groups, in MIBC. Moreover, reduced JCHAIN expression has been associated with unfavourable outcomes in solid tumours, both in pan-cancer analyses, where high expression correlates with favourable prognosis across most tumour types[121], and in breast cancer, where reduced expression at both transcript and protein level was associated with poorer prognosis and with the composition of the immune infiltrate[122]. If the reduction we observe reflects a genuine decrease in the output of multimeric immunoglobulin, it would suggest that the functional consequence of the shift described above is a loss of humoral effector capacity. The downregulation of B cell receptor signalling observed in the same pathway analysis is relevant in this context, since BCR engagement provides the initiating signal for B cell activation and differentiation[123]. Finally, interaction prediction analysis revealed how interactions between tumour and almost all B cells are increased in MIBC compared with NMIBC. It is also of interest that the most prominent shifts with the tumour as a sender involved all plasma cell and plasmablast clusters. Exposure of naive

splenic B cells to MB49 conditioned medium further supported our hypothesis, since it reduced the frequency of plasma cells. When plasma cell differentiation was actively driven by LPS or CD40L, the addition of conditioned medium consistently reduced the resulting plasma cell frequency, in some conditions to levels at or below those of unstimulated controls. Plasma cells and mature B cells were also reduced in BBN-treated animals at the late, MIBC-like time point. CXCR4 upregulation emerged as the most consistent finding of this work. It was among the most upregulated genes in MIBC B cells, the CXCR4 pathway was among the enriched ones in the same comparison, B cells showed the strongest CXCR4 upregulation of any population in the dataset, and exposure to conditioned medium *in vitro* induced the receptor to a degree greater than any other change measured in that experiment. At first sight, high CXCR4 and impaired B cell differentiation appear discordant, since CXCR4 induction is a canonical feature of the plasma cell programme[124], and is required for the homing and retention of plasma cells within survival niches[124]. One way of reconciling the two observations is to propose that plasma cell differentiation is initiated but not completed. Induction of CXCR4 coupled with reduced JCHAIN and N-glycosylation would correspond to cells that have entered the programme and accumulated at intermediate stages rather than progressing to functional antibody-secreting cells. To this extent, Biajoux et al.[125] generated a knock-in model of WHIM syndrome, in which gain-of-function mutations impair CXCR4 desensitisation. Sustained CXCR4 signalling counter-intuitively inhibited the maintenance of antibody responses, with plasma cell differentiation promoted locally but antigen-specific plasma cells almost absent from the bone marrow and with an early accumulation of immature plasmablasts. This led the authors to conclude that fine-tuning of CXCR4 desensitisation is required for efficient plasma cell differentiation. It must be noted, though, that this model recapitulates a genetic immunodeficiency rather than a tumour, and therefore can only establish a mechanistic precedent. In the tumour context, the closest comparable observation comes from gastric cancer, where combined single-cell and bulk analysis with immunohistochemical validation showed that CXCR4 expression in tumour-infiltrating B cells correlates with active, immature and memory B cell populations and that elevated CXCR4 is associated with worse overall survival[126]. This interpretation should nonetheless be held alongside alternatives, since the CXCR4 phenotype may not be linked to the differentiation phenotype at all. A first consideration

in this sense is that CXCR4 was upregulated in MIBC across most populations of the dataset, not only in B cells. Although the magnitude of the change was greatest in B cells, a shift affecting the microenvironment as a whole may be caused by a shared environmental input rather than a lineage-specific programme. The most obvious candidate is hypoxia, which is more pronounced in invasive tumours and is a well-established transcriptional inducer of CXCR4: the von Hippel-Lindau protein negatively regulates CXCR4 by targeting HIF for degradation. This process is inhibited during hypoxic conditions, leading to CXCR4 activation in a HIF-dependent manner[127,128]. Then, CXCR4 primarily governs positioning and retention, so its upregulation may also reflect altered trafficking or retention of B cells within the tumour[129,130], independently of their maturation state. The model proposed above is therefore offered as the interpretation that accounts for the largest number of our observations, not as the only one compatible with them. An alternative interpretation of the differences in plasma cells also deserves consideration, because a reduced plasma cell output is not always detrimental. Blocking the plasma cell fate genetically, either by preventing antibody secretion or by B cell-specific deletion of Blimp-1, was recently shown to promote rather than inhibit antitumour immunity, increasing the number of activated B cells and generating a transcriptional profile associated with expansion of tumour-reactive clones[131]. MHC class II was required for this effect. The mechanistic basis is that terminal plasma cell differentiation causes loss of antigen-presenting capacity, while B cells prevented from completing it remain available as antigen-presenting and co-stimulatory cells. This is consistent with one of our own observations, since MHC class II expression was increased in B cells exposed to tumour-conditioned medium *in vitro*. However, the *in vivo* data did not support the antigen-presenting reading, since the proportion of MHC class II-high B cells was reduced, not increased, in BBN-treated animals at the late time point, in the opposite direction to the *in vitro* result. Finally, a possibility for future experiments could be investigation of tertiary lymphoid structure (TLS) presence, location, and maturation in NMIBC and MIBC patients' tissues. TLSs are ectopic lymphoid aggregates that arise in chronically inflamed tissues, including tumours, where they have been associated with improved prognosis and enhanced responsiveness to immunotherapy, highlighting their potential as both predictive biomarkers and functional immune niches[132]. They are known to be present in many types of cancers, where they are associated with good prognosis[67].

Moreover, recent spatial transcriptomics analysis coupled with spatial proteomics of 12 different cancer types, including bladder cancer, revealed how TLS maturation and proximity to tumour are strong predictors of overall survival and response to chemotherapy and targeted therapy[133]. Analyses of tertiary lymphoid structure formation in this context are ongoing and will be reported separately, but they are not included in this thesis. Finally, it is important to mention the limitations related to this work. The papilloma group comprised only two samples, and all comparisons involving this group should be regarded as indicative. Also, the cell population proportions from the scRNA-seq analysis carry the compositional caveats discussed above. The CellChat analysis infers rather than measures intercellular communication, and its output depends on the curated ligand-receptor database used. The predicted interactions reported here should be regarded as hypotheses to be tested rather than as established signalling events. The *in vitro* system is based on conditioned medium from a single murine bladder cancer cell line, whose secretome was not characterised. The factor or factors responsible for CXCR4 induction and for the differentiation block therefore remain unidentified. In addition, splenic B cells from tumour-free mice are not equivalent to tumour-infiltrating B cells in patients, both in their prior activation history and in the duration of their exposure to tumour-derived signals. Also, the choice of adopting an experimental strategy using tumour-conditioned medium is a double-edged sword: on one hand, it provides a focus specifically on changes induced by factors secreted by the tumour, recapitulating the effects of the tumour microenvironment on B cells, but on the other hand it fails to recapitulate all interactions that require direct contact. The *in vivo* model reproduced part, but not all, of the phenotype. The reduction of plasma cells was recapitulated, whereas the reduction of mature B cells and the redistribution within the transitional compartment tracked with time point rather than with carcinogen treatment, and the functional markers behaved differently from the *in vitro* system. These differences reflect the biological differences between an isolated culture system and an organism in which B cells develop, traffic and encounter the tumour within a complete immune network.

CONCLUSIONS AND FUTURE PERSPECTIVES

This work provides a characterisation of the immune microenvironment of bladder cancer across the non-invasive-to-invasive transition, and identifies the B cell compartment as the site of the most consistent alterations. Across three independent systems, we find convergent evidence that the differentiation of B cells towards antibody-secreting cells is impaired in muscle-invasive disease, accompanied by downregulation of the transcriptional programmes required for immunoglobulin assembly and secretion. CXCR4 emerges as the most prominent candidate associated with this phenotype. Its upregulation in patient B cells, its strong induction by conditioned medium, and the existence of a published mechanism whereby dysregulated CXCR4 signalling arrests plasma cell maturation at immature stages together support the hypothesis that sustained CXCR4 signalling contributes to an initiated but incomplete differentiation programme. This hypothesis is, at present, supported by association rather than by causal evidence. Beyond this, three further directions arise. First, characterisation of the MB49 secretome would identify the soluble factor responsible for the phenotype. Second, an experimental setup allowing direct contact between B cells and tumour cells would address the contact-dependent component of the interaction, which the conditioned medium approach leaves unexplored. Finally, the analyses of tertiary lymphoid structures currently underway in this cohort will indicate whether the alterations described here are accompanied by changes in the organisation and maturation of the structures within which B cell responses are coordinated.

BIBLIOGRAPHY

1. Bazira, P. J. Anatomy of the lower urinary tract. *Surg. Oxf.* **40**, 489–500 (2022).

2. Sánchez Freire, V., Burkhard, F. C., Schmitz, A., Kessler, T. M. & Monastyrskaya, K. Structural differences between the bladder dome and trigone revealed by mRNA expression analysis of cold-cut biopsies. *BJU Int.* **108**, E126–E135 (2011).

3. Hicks, R. M. The Mammalian Urinary Bladderan Accommodating Organ. *Biol. Rev.* **50**, 215–246 (1975).

4. Shin, K. *et al.* Hedgehog/Wnt feedback supports regenerative proliferation of epithelial stem cells in bladder. *Nature* **472**, 110–114 (2011).

5. Jafari, N. V. & Rohn, J. L. The urothelium: a multi-faceted barrier against a harsh environment. *Mucosal Immunol.* **15**, 1127–1142 (2022).

6. Balsara, Z. R. & Li, X. Sleeping beauty: awakening urothelium from its slumber. *Am. J. Physiol.-Ren. Physiol.* **312**, F732–F743 (2017).

7. Khandelwal, P., Abraham, S. N. & Apodaca, G. Cell biology and physiology of the uroepithelium. *Am. J. Physiol.-Ren. Physiol.* **297**, F1477–F1501 (2009).

8. Dalghi, M. G., Montalbetti, N., Carattino, M. D. & Apodaca, G. The Urothelium: Life in a Liquid Environment. *Physiol. Rev.* **100**, 1621–1705 (2020).

9. Wu, X.-R., Kong, X.-P., Pellicer, A., Kreibich, G. & Sun, T.-T. Uroplakins in Urothelial Biology, Function and Disease. *Kidney Int.* **75**, 1153–1165 (2009).

10. Bray, F. *et al.* Global cancer statistics 2022: GLOBOCAN estimates of incidence and mortality worldwide for 36 cancers in 185 countries. *CA. Cancer J. Clin.* **74**, 229–263 (2024).

11. Taylor, J. A. & Kuchel, G. A. Bladder cancer in the elderly: clinical outcomes, basic mechanisms, and future research direction. *Nat. Clin. Pract. Urol.* **6**, 135–144 (2009).

12. Saginala, K. *et al.* Epidemiology of Bladder Cancer. *Med. Sci.* **8**, 15 (2020).

13. Halaseh, S. A., Halaseh, S., Alali, Y., Ashour, M. E. & Alharayzah, M. J. A Review of the Etiology and Epidemiology of Bladder Cancer: All You Need To Know. *Cureus* **14**, e27330.

14. Kwan, M. L., Garren, B., Nielsen, M. E. & Tang, L. Lifestyle and Nutritional Modifiable Factors in the Prevention and Treatment of Bladder Cancer. *Urol. Oncol.* **37**, 380–386 (2019).
15. Slaughter, D. P., Southwick, H. W. & Smejkal, W. Field cancerization in oral stratified squamous epithelium; clinical implications of multicentric origin. *Cancer* **6**, 963–968 (1953).
16. Curtius, K., Wright, N. A. & Graham, T. A. An evolutionary perspective on field cancerization. *Nat. Rev. Cancer* **18**, 19–32 (2018).
17. Papafotiou, G. *et al.* KRT14 marks a subpopulation of bladder basal cells with pivotal role in regeneration and tumorigenesis. *Nat. Commun.* **7**, 11914 (2016).
18. AJCC Cancer Staging Manual | Springer Nature Link. https://link.springer.com/book/9783319406176?
19. Witjes, J. A. *et al.* European Association of Urology Guidelines on Muscle-invasive and Metastatic Bladder Cancer: Summary of the 2020 Guidelines. *Eur. Urol.* **79**, 82–104 (2021).
20. Babjuk, M. *et al.* European Association of Urology Guidelines on Non–muscle-invasive Bladder Cancer (Ta, T1, and Carcinoma in Situ). *Eur. Urol.* **81**, 75–94 (2022).
21. Survival of patients with carcinoma in situ of the urinary bladder - Cheng - 1999 - Cancer - Wiley Online Library. https://acsjournals.onlinelibrary.wiley.com/doi/10.1002/(SICI)1097-0142(19990601)85:11%3C2469::AID-CNCR24%3E3.0.CO;2-U.
22. The genetics of transitional cell carcinoma: progress and potential clinical application. https://bjui-journals.onlinelibrary.wiley.com/doi/epdf/10.1046/j.1464-410x.1999.00217.x.
23. Inverted papilloma of the bladder: A review and an analysis of the recent literature of 365 patients - ScienceDirect. https://www.sciencedirect.com/science/article/pii/S1078143912000907?via%3Dihub.
24. Telloni, S. M. Tumor Staging and Grading: A Primer. in *Molecular Profiling: Methods and Protocols* (ed. Espina, V.) 1–17 (Springer, New York, NY, 2017). doi:10.1007/978-1-4939-6990-6_1.

25. . Pathology and genetics of tumours of the urinary... - Google Scholar. https://scholar.google.com/scholar?q=.+Pathology+and+genetics+of+tumours+of+the+urinary+system+and+male+genital+organs.+Lyon%3A+IARC+Press%2C+2004.
26. Molecular Pathogenesis and Diagnostics of Bladder Cancer | Annual Reviews. https://www.annualreviews.org/content/journals/10.1146/annurev.pathol.4.110807.092230.
27. Mutational landscape of non-muscle-invasive bladder cancer - ScienceDirect. https://www.sciencedirect.com/science/article/pii/S1078143918303983?via%3Dihub#abs0001.
28. T1 bladder cancer: current considerations for diagnosis and management | Nature Reviews Urology. https://www.nature.com/articles/s41585-018-0105-y.
29. Hurst, C. D. *et al.* Stage-stratified molecular profiling of non-muscle-invasive bladder cancer enhances biological, clinical, and therapeutic insight. *Cell Rep. Med.* **2**, 100472 (2021).
30. Barski, D. The arguments for an early cystectomy in patients with urothelial carcinoma. *Cent. Eur. J. Urol.* **67**, 333–334 (2014).
31. Arruda, J. B. & Salkini, M. W. Is radical cystectomy an overtreatment for T1 high-grade transitional cell carcinoma of the bladder? Lesson learnt from case series. *Urol. Ann.* **13**, 326–328 (2021).
32. Preventable Cancer Deaths Associated with Bladder Preservation for Muscle Invasive Bladder Cancer - PubMed. https://pubmed.ncbi.nlm.nih.gov/31071350/.
33. HER2/neu overexpression in the development of muscle-invasive transitional cell carcinoma of the bladder | British Journal of Cancer. https://www.nature.com/articles/6601245.
34. Staging of bladder cancer - Magers - 2019 - Histopathology - Wiley Online Library. https://onlinelibrary.wiley.com/doi/10.1111/his.13734.
35. Shankar, P. R., Barkmeier, D., Hadjiiski, L. & Cohan, R. H. A pictorial review of bladder cancer nodal metastases. *Transl. Androl. Urol.* **7**, 804–813 (2018).
36. Owen, J., Punt, J. & Stranford, S. A. *Kuby Immunology*.
37. Mittal, D., Gubin, M. M., Schreiber, R. D. & Smyth, M. J. New insights into cancer immunoediting and its three component phases--elimination, equilibrium and escape. *Curr. Opin. Immunol.* **27**, 16–25 (2014).

38. de Visser, K. E. & Joyce, J. A. The evolving tumor microenvironment: From cancer initiation to metastatic outgrowth. *Cancer Cell* **41**, 374–403 (2023).
39. The dynamic roles of the bladder tumour microenvironment | Nature Reviews Urology. https://www.nature.com/articles/s41585-022-00608-y.
40. Yang, D., Liu, J., Qian, H. & Zhuang, Q. Cancer-associated fibroblasts: from basic science to anticancer therapy. *Exp. Mol. Med.* **55**, 1322–1332 (2023).
41. Reactive stroma in human prostate cancer: induction of myofibroblast phenotype and extracellular matrix remodeling - PubMed. https://pubmed.ncbi.nlm.nih.gov/12231536/.
42. A framework for advancing our understanding of cancer-associated fibroblasts | Nature Reviews Cancer. https://www.nature.com/articles/s41568-019-0238-1.
43. Peng, D., Fu, M., Wang, M., Wei, Y. & Wei, X. Targeting TGF-β signal transduction for fibrosis and cancer therapy. *Mol. Cancer* **21**, 104 (2022).
44. Camorani, S. *et al.* Inhibition of Bone Marrow-Derived Mesenchymal Stem Cells Homing Towards Triple-Negative Breast Cancer Microenvironment Using an Anti-PDGFRβ Aptamer. *Theranostics* **7**, 3595–3607 (2017).
45. Martinez-Outschoorn, U. E. *et al.* Oxidative stress in cancer associated fibroblasts drives tumor-stroma co-evolution. *Cell Cycle* **9**, 3256–3276 (2010).
46. Díaz-Maroto, N. G. *et al.* The Blockade of Tumoral IL1β-Mediated Signaling in Normal Colonic Fibroblasts Sensitizes Tumor Cells to Chemotherapy and Prevents Inflammatory CAF Activation. *Int. J. Mol. Sci.* **22**, 4960 (2021).
47. The biology and function of fibroblasts in cancer | Nature Reviews Cancer. https://www.nature.com/articles/nrc.2016.73.
48. Gomes, R. N., Manuel, F. & Nascimento, D. S. The bright side of fibroblasts: molecular signature and regenerative cues in major organs. *Npj Regen. Med.* **6**, 43 (2021).
49. Fibroblasts in urothelial bladder cancer define stroma phenotypes that are associated with clinical outcome | Scientific Reports. https://www.nature.com/articles/s41598-019-55013-0.
50. Shen, J. *et al.* CCL5 promotes the proliferation and metastasis of bladder cancer via the JAK2/STAT3 signaling pathway. *Transl. Androl. Urol.* **12**, 1845–1858 (2023).

51. Liang, T. *et al.* Cancer-Associated Fibroblast-Induced Remodeling of Tumor Microenvironment in Recurrent Bladder Cancer. *Adv. Sci.* **10**, 2303230 (2023).
52. Wang, M. *et al.* The research advances of crosstalk between cancer-associated fibroblasts and tumor cells using co-culture organoids. *Cell Death Dis.* **17**, 267 (2026).
53. Szarvas, T., vom Dorp, F., Ergün, S. & Rübben, H. Matrix metalloproteinases and their clinical relevance in urinary bladder cancer. *Nat. Rev. Urol.* **8**, 241–254 (2011).
54. Mariathasan, S. *et al.* TGFβ attenuates tumour response to PD-L1 blockade by contributing to exclusion of T cells. *Nature* **554**, 544–548 (2018).
55. Hashitani, H., Mitsui, R., Shimizu, Y., Higashi, R. & Nakamura, K. Functional and morphological properties of pericytes in suburothelial venules of the mouse bladder. *Br. J. Pharmacol.* **167**, 1723–1736 (2012).
56. Fukumura, D. & Jain., R. K. Tumor microvasculature and microenvironment: Targets for anti-angiogenesis and normalization. *Microvasc. Res.* **74**, 72–84 (2007).
57. Patel, N. S. *et al.* Up-Regulation of Endothelial Delta-like 4 Expression Correlates with Vessel Maturation in Bladder Cancer. *Clin. Cancer Res.* **12**, 4836–4844 (2006).
58. John, A. *et al.* Urothelial Carcinoma of the Bladder Induces Endothelial Cell Activation and Hypercoagulation. *Mol. Cancer Res.* **18**, 1099–1109 (2020).
59. Kraja, F. P. *et al.* Tumor-infiltrating lymphocytes in cancer immunotherapy: from chemotactic recruitment to translational modeling. *Front. Immunol.* **16**, (2025).
60. Liakou, C. I., Narayanan, S., Ng Tang, D., Logothetis, C. J. & Sharma, P. Focus on TILs: Prognostic significance of tumor infiltrating lymphocytes in human bladder cancer. *Cancer Immun. J. Acad. Cancer Immunol.* **7**, 10 (2007).
61. Sheu, B. C. *et al.* Predominant Th2/Tc2 polarity of tumor-infiltrating lymphocytes in human cervical cancer. *J. Immunol.* **167**, 2972–2978 (2001).
62. Fu, C. & Jiang, A. Dendritic Cells and CD8 T Cell Immunity in Tumor Microenvironment. *Front. Immunol.* **9**, 3059 (2018).
63. Yang, H. *et al.* The Dual Role of B Cells in the Tumor Microenvironment: Implications for Cancer Immunology and Therapy. *Int. J. Mol. Sci.* **25**, 11825 (2024).
64. Rastogi, I. *et al.* Role of B cells as antigen presenting cells. *Front. Immunol.* **13**, 954936 (2022).

65. Jiang, Y., Zhang, Q., Yang, Z., Yang, K. & Zhou, S. The multifaceted roles of tumor-infiltrating plasma cells in cancer immunology. *Fundam. Res.* https://doi.org/10.1016/j.fmre.2025.12.009 (2025) doi:10.1016/j.fmre.2025.12.009.

66. Janjic, B. M., Kulkarni, A., Ferris, R. L., Vujanovic, L. & Vujanovic, N. L. Human B Cells Mediate Innate Anti-Cancer Cytotoxicity Through Concurrent Engagement of Multiple TNF Superfamily Ligands. *Front. Immunol.* **13**, 837842 (2022).

67. Sautès-Fridman, C. *et al.* Tertiary Lymphoid Structures in Cancers: Prognostic Value, Regulation, and Manipulation for Therapeutic Intervention. *Front. Immunol.* **7**, (2016).

68. Junt, T., Scandella, E. & Ludewig, B. Form follows function: lymphoid tissue microarchitecture in antimicrobial immune defence. *Nat. Rev. Immunol.* **8**, 764–775 (2008).

69. Fridman, W. H., Zitvogel, L., Sautès-Fridman, C. & Kroemer, G. The immune contexture in cancer prognosis and treatment. *Nat. Rev. Clin. Oncol.* **14**, 717–734 (2017).

70. From the MRC Centre for Transplantation, King's College London School of Medicine at Guy's, King's and St. Thomas' Hospitals, London, United Kingdom *et al.* Characterizing the B-Cell and Humoral Response in Tertiary Lymphoid Organs in Kidney Allografts. *Exp. Clin. Transplant.* **17**, 330–338 (2019).

71. Joshi, N. S. *et al.* Regulatory T Cells in Tumor-Associated Tertiary Lymphoid Structures Suppress Anti-tumor T Cell Responses. *Immunity* **43**, 579–590 (2015).

72. Li, Z. *et al.* Multiple mechanisms and applications of tertiary lymphoid structures and immune checkpoint blockade. *J. Exp. Clin. Cancer Res. CR* **44**, 84 (2025).

73. Chekol Abebe, E. *et al.* The Role of Regulatory B Cells in Health and Diseases: A Systemic Review. *J. Inflamm. Res.* **14**, 75–84 (2021).

74. Cai, Z. & Xie, L. Regulatory B Cells in Tumor Microenvironment. *Curr. Issues Mol. Biol.* **48**, 106 (2026).

75. Zhong, Z. *et al.* Pro- and Anti- Effects of Immunoglobulin A- Producing B Cell in Tumors and Its Triggers. *Front. Immunol.* **12**, 765044 (2021).

76. Dyugay, I. A. *et al.* Accounting for B-cell Behavior and Sampling Bias Predicts Anti–PD-L1 Response in Bladder Cancer. *Cancer Immunol. Res.* **10**, 343–353 (2022).
77. Yuan, H. *et al.* Single-cell sequencing reveals the heterogeneity of B cells and tertiary lymphoid structures in muscle-invasive bladder cancer. *J. Transl. Med.* **22**, 48 (2024).
78. Dyugay, I. A. *et al.* Accounting for B-cell Behavior and Sampling Bias Predicts Anti-PD-L1 Response in Bladder Cancer. *Cancer Immunol. Res.* **10**, 343–353 (2022).
79. Racacho, K. J. *et al.* The tumor immune microenvironment: implications for cancer immunotherapy, treatment strategies, and monitoring approaches. *Front. Immunol.* **16**, 1621812 (2025).
80. Pere, H. *et al.* A CCR4 antagonist combined with vaccines induces antigen-specific CD8+ T cells and tumor immunity against self antigens. *Blood* **118**, 4853–4862 (2011).
81. Henze, A.-T. & Mazzone, M. The impact of hypoxia on tumor-associated macrophages. *J. Clin. Invest.* **126**, 3672–3679 (2016).
82. Chen, Y. *et al.* Tumor-associated macrophages: an accomplice in solid tumor progression. *J. Biomed. Sci.* **26**, 78 (2019).
83. Mantovani, Alberto, Sica, Antonio & Locati, M. Macrophage Polarization Comes of Age. *Immunity* **23**, 344–346 (2005).
84. Wang, H.-Y. *et al.* Ratios of CD8 T lymphocytes to M-MDSCs (CD8MMR) predict prognosis in patients with untreated DLBCL. *Blood Neoplasia* **3**, 100180 (2025).
85. Wu, B., Zhang, B., Li, B., Wu, H. & Jiang, M. Cold and hot tumors: from molecular mechanisms to targeted therapy. *Signal Transduct. Target. Ther.* **9**, 274 (2024).
86. Richterstetter, M. *et al.* The value of extended transurethral resection of bladder tumour (TURBT) in the treatment of bladder cancer. *BJU Int.* **110**, E76–E79 (2012).
87. Nerli, R. B. *et al.* Low-Grade, Multiple, Ta Non-muscle-Invasive Bladder Tumors: Tumor Recurrence and Worsening Progression. *Indian J. Surg. Oncol.* **9**, 157–161 (2018).
88. Morales, A., Eidinger, D. & Bruce, A. W. Intracavitary Bacillus Calmette-Guerin in the treatment of superficial bladder tumors. *J. Urol.* **116**, 180–183 (1976).

89. LUCA, S. & MIHAESCU, T. History of BCG Vaccine. *Mædica* **8**, 53–58 (2013).
90. Böhle, A. & Bock, P. R. Intravesical bacille calmette-guérin versus mitomycin c in superficial bladder cancer: formal meta-analysis of comparative studies on tumor progression. *Urology* **63**, 682–686 (2004).
91. Redelman-Sidi, G., Glickman, M. S. & Bochner, B. H. The mechanism of action of BCG therapy for bladder cancer--a current perspective. *Nat. Rev. Urol.* **11**, 153–162 (2014).
92. Grimm, M.-O. *et al.* Treatment of High-grade Non–muscle-invasive Bladder Carcinoma by Standard Number and Dose of BCG Instillations Versus Reduced Number and Standard Dose of BCG Instillations: Results of the European Association of Urology Research Foundation Randomised Phase III Clinical Trial "NIMBUS". *Eur. Urol.* **78**, 690–698 (2020).
93. van der Meijden, A. P. M., Sylvester, R. J., Oosterlinck, W., Hoeltl, W. & Bono, A. V. Maintenance Bacillus Calmette-Guerin for Ta T1 Bladder Tumors Is Not Associated with Increased Toxicity: Results from a European Organisation for Research and Treatment of Cancer Genito-Urinary Group Phase III Trial. *Eur. Urol.* **44**, 429–434 (2003).
94. Cambier, S. *et al.* EORTC Nomograms and Risk Groups for Predicting Recurrence, Progression, and Disease-specific and Overall Survival in Non-Muscle-invasive Stage Ta-T1 Urothelial Bladder Cancer Patients Treated with 1-3 Years of Maintenance Bacillus Calmette-Guérin. *Eur. Urol.* **69**, 60–69 (2016).
95. Bajorin, D. F. *et al.* Adjuvant Nivolumab versus Placebo in Muscle-Invasive Urothelial Carcinoma. *N. Engl. J. Med.* **384**, 2102–2114 (2021).
96. Ishida, Y., Agata, Y., Shibahara, K. & Honjo, T. Induced expression of PD-1, a novel member of the immunoglobulin gene superfamily, upon programmed cell death. *EMBO J.* **11**, 3887–3895 (1992).
97. Patel, A. *et al.* Immune Checkpoint Inhibitors in the Management of Urothelial Carcinoma. *J. Cancer Immunol.* **3**, 115–136 (2021).
98. Steinmetz, A. R., Mokkapati, S., McConkey, D. & Dinney, C. P. The Evolution of Nadofaragene Firadenovec: A Review and the Path Forward. *Bladder Cancer* **10**, 105–112 (2024).

99. MohanaSundaram, A., Raja, V., Kamalakannan, Y. & Islam, M. A. Nogapendekin alfa Inbakicept-pmln (Anktiva) with BCG: A Promising Arsenal in BCG-Unresponsive Non-Muscle-Invasive Bladder Cancer Intervention. *Adv. Pharm. Bull.* **15**, 4–6.
100. Research, C. for D. E. and. FDA approves durvalumab in combination with Bacillus Calmette-Guerin for high-risk non-muscle invasive bladder cancer. *FDA* https://www.fda.gov/drugs/resources-information-approved-drugs/fda-approves-durvalumab-combination-bacillus-calmette-guerin-high-risk-non-muscle-invasive-bladder (2026).
101. Adjuvant Nivolumab versus Placebo in Muscle-Invasive Urothelial Carcinoma | New England Journal of Medicine. https://www.nejm.org/doi/full/10.1056/NEJMoa2034442.
102. Research, C. for D. E. and. FDA approves pembrolizumab or pembrolizumab and berahyaluronidase alfa-pmph each with enfortumab vedotin-ejfv for muscle invasive bladder cancer. *FDA* https://www.fda.gov/drugs/resources-information-approved-drugs/fda-approves-pembrolizumab-or-pembrolizumab-and-berahyaluronidase-alfa-pmph-each-enfortumab-vedotin (2026).
103. Research, C. for D. E. and. FDA approves atezolizumab for adjuvant treatment of muscle invasive bladder cancer in patients with molecular residual disease. *FDA* https://www.fda.gov/drugs/resources-information-approved-drugs/fda-approves-atezolizumab-adjuvant-treatment-muscle-invasive-bladder-cancer-patients-molecular (2026).
104. Váradi, M. *et al.* Prognostic and predictive factors of immune checkpoint inhibitor therapy in urinary bladder cancer. *Pathol. Oncol. Res. POR* **32**, 1612333 (2026).
105. de Jong, F. C. *et al.* PD-L1 expression in high-risk non-muscle invasive bladder cancer is not a biomarker of response to BCG. *World J. Urol.* **43**, 57 (2025).
106. Kocsmár, I. *et al.* Addition of Chromosome 17 Polysomy and HER2 Amplification Status Improves the Accuracy of Clinicopathological Factor-Based Progression Risk Stratification and Tumor Grading of Non-Muscle-Invasive Bladder Cancer. *Cancers* **14**, 4570 (2022).

107. N, S. *et al.* Novel Gene expression-based Risk Stratification tool predicts recurrence in Non-muscle invasive Bladder cancer. *BMC Cancer* **25**, 916 (2025).
108. Tran, L., Xiao, J.-F., Agarwal, N., Duex, J. E. & Theodorescu, D. Advances in bladder cancer biology and therapy. *Nat. Rev. Cancer* **21**, 104–121 (2021).
109. Daza, J., Charap, A., Wiklund, P. N. & Sfakianos, J. P. Role of the Innate Immune System in the Development, Progression, and Therapeutic Response of Bladder Cancer. *Eur. Urol. Focus* **6**, 650–652 (2020).
110. Penunuri, A., Greenberg, E., Phillips, J. & Katims, A. B. The Emerging Role of B Cells and Tertiary Lymphoid Structures in Bladder Cancer. *Curr. Urol. Rep.* **27**, 3 (2025).
111. Marth, J. D. & Prabhjit, G. K. Mammalian glycosylation in immunity. (2008).
112. Penunuri, A., Greenberg, E., Phillips, J. & Katims, A. B. The Emerging Role of B Cells and Tertiary Lymphoid Structures in Bladder Cancer. *Curr. Urol. Rep.* **27**, 3 (2025).
113. Hartana, C. A. *et al.* Tissue-resident memory T cells are epigenetically cytotoxic with signs of exhaustion in human urinary bladder cancer. *Clin. Exp. Immunol.* **194**, 39–53 (2018).
114. Dyrskjøt, L. *et al.* Bladder cancer. *Nat. Rev. Dis. Primer* **9**, 58 (2023).
115. Li, B. *et al.* Integrating molecular subtype and CD8+ T cells infiltration to predict treatment response and survival in muscle-invasive bladder cancer. *Cancer Immunol. Immunother. CII* **73**, 66 (2024).
116. Hassan, W. A. *et al.* Significance of tumor-associated neutrophils, lymphocytes, and neutrophil-to-lymphocyte ratio in non-invasive and invasive bladder urothelial carcinoma. *J. Pathol. Transl. Med.* **57**, 88–94 (2023).
117. Squair, J. W. *et al.* Confronting false discoveries in single-cell differential expression. *Nat. Commun.* **12**, 5692 (2021).
118. Phipson, B. *et al.* propeller: testing for differences in cell type proportions in single cell data. *Bioinformatics* **38**, 4720–4726 (2022).
119. Yang, Y. *et al.* Pan-cancer single-cell dissection reveals phenotypically distinct B cell subtypes. *Cell* **187**, 4790-4811.e22 (2024).

120. van de Bovenkamp, F. S. *et al.* Adaptive antibody diversification through N-linked glycosylation of the immunoglobulin variable region. *Proc. Natl. Acad. Sci.* **115**, 1901–1906 (2018).
121. JCHAIN: A Prognostic Marker Based on Pan-Cancer Analysis to Inhibit Breast Cancer Progression. https://www.mdpi.com/2073-4425/16/9/1070.
122. Hu, Y. *et al.* Construction and evaluation of a prognostic model for breast cancer based on aging related genes. *Sci. Rep.* **15**, 33756 (2025).
123. Akkaya, M., Kwak, K. & Pierce, S. K. B cell memory: building two walls of protection against pathogens. *Nat. Rev. Immunol.* **20**, 229–238 (2020).
124. Muehlinghaus, G. *et al.* Regulation of CXCR3 and CXCR4 expression during terminal differentiation of memory B cells into plasma cells. *Blood* **105**, 3965–3971 (2005).
125. Biajoux, V. *et al.* Efficient Plasma Cell Differentiation and Trafficking Require Cxcr4 Desensitization. *Cell Rep.* **17**, 193–205 (2016).
126. Su, C. *et al.* CXCR4 Expressed by Tumor-Infiltrating B Cells in Gastric Cancer Related to Survival in the Tumor Microenvironment: An Analysis Combining Single-Cell RNA Sequencing with Bulk RNA Sequencing. *Int. J. Mol. Sci.* **24**, 12890 (2023).
127. Staller, P. *et al.* Chemokine receptor CXCR4 downregulated by von Hippel-Lindau tumour suppressor pVHL. *Nature* **425**, 307–311 (2003).
128. Jang, J.-W., Thuy, P. X., Lee, J.-W. & Moon, E.-Y. CXCR4 promotes B cell viability by the cooperation of nuclear factor (erythroid-derived 2)-like 2 and hypoxia-inducible factor-1α under hypoxic conditions. *Cell Death Dis.* **12**, 330 (2021).
129. Allen, C. D. C. *et al.* Germinal center dark and light zone organization is mediated by CXCR4 and CXCR5. *Nat. Immunol.* **5**, 943–952 (2004).
130. Sugiyama, T., Kohara, H., Noda, M. & Nagasawa, T. Maintenance of the hematopoietic stem cell pool by CXCL12-CXCR4 chemokine signaling in bone marrow stromal cell niches. *Immunity* **25**, 977–988 (2006).
131. Li, Y. *et al.* Blocking plasma cell fate enhances antigen-specific presentation by B cells to boost anti-tumor immunity. *Nat. Commun.* **16**, 4454 (2025).
132. Teillaud, J.-L., Houel, A., Panouillot, M., Riffard, C. & Dieu-Nosjean, M.-C. Tertiary lymphoid structures in anticancer immunity. *Nat. Rev. Cancer* **24**, 629–646 (2024).

133. Pan-cancer spatial atlas of tertiary lymphoid structures | Science. https://www.science.org/doi/10.1126/science.adz2742.